LUNDS UNIVERSITET

Mechanical properties of SiC nanowires with polytypes

ANDERS VESTI

Thesis submitted for the degree of Master of Science
Project Duration: 5 months

Supervised by

JONAS JOHANSSON and
PER HANSSON

Department of Physics
Division of Solid State Physics
May 2019

Abstract

In this report, we model the mechanical properties and fracture behavior of SiC nanowires with different polytypes using Molecular Dynamics (MD) simulations. The mechanical properties investigated are the Young's modulus, the maximum tensile stress and the fracture strain. The three polytype tested are SiC (3C), (2H) and (4H). Tensile tests are performed on bulk and nanowire samples using three commonly know inter-atomic potentials: the Tersoff, the Vashishta and the MEAM potential. Our report finds large differences in how the potentials predict the mechanical properties and fracture behavior of the SiC structures.

Using the MEAM potential, we perform tests on two similar sized nanowires with different side facets: one with {11-2} surfaces and one with {1-10} surfaces. The surface energies of the two surface types are estimated. Our studies find that the type of surfaces will affect the mechanical properties of the nanowire.

The mechanical properties of the three SiC polytypes are obtained at four different temperatures. A dependence of the Young's modulus on the hexagonality of unit cell is found, a dependence also reported for diamond polytypes. We further find that increasing temperatures will lower the values of the mechanical properties.

Lastly, two nanowire heterostructures are constructed using diamond cubic Si and either SiC (3C) and SiC (2H). The potential energy of the interface is estimated and compared to the Si and SiC (3C)/(2H) sections of the heterostructure. We find that due to dislocations the energy is highest at the interface. The dislocation pattern of the interface is analyzed, and edge dislocations of the type $\frac{1}{2}\langle 110\rangle$ and $\frac{1}{6}\langle$11-2$\rangle$ are found.

Acknowledgment

I would like to thank my two supervisors Jonas Johansson and Per Hansson for their supervision and counseling which has been a great help in writing this report. I also thank Pär Olsson for his expertise and advice which has been greatly helpful during my work.

Lastly, I want to thank my family and friends for their support and patience with me during my thesis work.

List of Abbreviations

BOA Born-Oppenheimer Approximation

DFT Density Functional Theory

EAM Embedded Atom Method

LAMMPS Large-scale Atomic/Molecular Massively Parallel Simulator

MD Molecular Dynamics

MEAM Modified Embedded Atom Method

SiC Silicon Carbide

wz Wurtzite

zb Zinc-blende

Contents

Introduction

The developments in the semiconductor industry and semiconductor device fabrication continues to grow with an incredible speed. The advancements in nanoscale device fabrication and the ever present demand of new solutions from the industry compel researchers to explore new semiconductor materials and device structures to create evermore specialized semiconductor devices.

A nanoscale structure that has sparked a lot of interest in recent years is the nanowire. Due to their low-dimension properties, it has been shown that nanowire based devices may bring several advances in various types of fields, for example as field effect transistors and optoelectronic devices.[1]

When it comes to the implementation of new semiconductor materials, Silicon carbide (SiC) posses physical properties that make it a strong candidate for creating highly specialized devices. Already now SiC has been used for making high power devices and devices that can withstand extreme temperatures. Furthermore, studies has shown that SiC nanowires can be grown using techniques already present in the semiconductor industry.[2] By producing SiC nanowires, we can combine the abilities of bulk SiC with the low-dimension properties of nanowires and thereby open the door to a whole new set of specialized devices.[2]

What further makes SiC an interesting material is that it exists as several polytypes. These polytypes do not only have different crystal structures, they also posses very different electronic properties. If scientist are able to fully control the formation of polytypes in SiC, it would allow us modify the electronic band structure of our devices using just one type of material; something that normally requires either adding a dopant or creating a heterostructure of two different types of materials.

In order to fully utilize SiC nanowires in future devices, scientists need to know their mechanical properties. Due to their small sizes, the mechanical properties of SiC nanowires are hard to obtain experimentally. Instead computer simulations are used, which allows us to test single polytype structures in a controlled and reproducible environment.

In this report we will use the computational method of Molecular Dynamics (MD) simulations to obtain the mechanical properties of the SiC nanowires. MD simulation is a technique that allows us to simulate the individual motion of each atom in a confined system.

The first computational MD simulations were carried out in the 1950's by researchers at Lawrence Livermore National Laboratory, where the trajectories of hundreds of hard sphere particles were computed using a simple square-well potential as inter-atomic potential.[3] Since then, the capabilities of MD simulations have grown as fast as the advancements in computer power, and today systems of many millions of atoms can be modeled. We will use the open-source software LAMMPS to perform the MD simulations, which is specialized in modeling solid materials.[4]

In MD simulations an inter-atomic potential needs to be specified. It is from this potential all the forces acting on each atom will be computed. This also indicates the limitations of MD simulations, since the results obtained are only as accurate as the inter-atomic potential. In our report we will test three commonly used inter-atomic potentials and compare the results with what is found in the literature to determine which potential is best suited for our studies.

SiC has more than 170 known polytypes.[5] These can be divided into groups depending on their hexagonality. We will limit ourselves to study three polytypes: SiC (3C) which has a cubic unit cell meaning 0% hexagonality, SiC (2H) which has a unit cell of 100% hexagonality, and SiC (4H) which can be seen as a mixture of the two former and has a hexagonality of 50%. Though these polytypes all exist in SiC nanowires, they are not necessarily commonly found.[6][7] However, we have chosen the polytypes not based on their prevalence but because of their scientific importance, since by choosing these three polytypes we capture the whole range of hexagonality from the highest to the lowest and one intermediate value.

Due to limited computational power available, we can only model nanowires of a limited diameter. The largest nanowires we simulate in this report have a diameter of $\sim$5 nm, while nanowires grown in the laboratory typically have diameters that are 10-20 times larger.[2] The smaller nanowires may cause any surface effects to be more prominent than nanowires of larger diameter.

The mechanical properties we obtain and compare for each SiC polytype are: the Young's modulus, the maximum stress and the fracture strain. Using the visualization tool Ovito, we are able to investigate the fracture behavior of the SiC nanowires. We will test the polytypes at four different temperatures to find the thermal dependency of the mechanical properties.

In this report, we will also create Si-SiC heterostructures and analyze the type of dislocations forming at the interface. Dislocations in nanowire heterostructures has previously been studied using other computational modeling methods, for example in the 2006 paper by F. Glas.[8] Here, it has to be assumed what type of dislocations will form. The advantage of MD simulations is that we do not need to make any assumption of what type of dislocations will form. We simply build the heterostructure and let it relax according to the inter-atomic potential.

This report will start by introducing the compound SiC and the three selected polytypes in Chapter 2. Chapter 3 is dedicated to introducing the theory behind and method of MD simulations, while Chapter 4 will introduce the three inter-atomic potentials: the Vashishta, the Tersoff, and the MEAM potential.

Chapter 5 will briefly introduce the different softwares used and show excerpts of our script developed to obtain the mechanical properties using MD simulations.

Our results are presented in Chapter 6 and lastly our conclusions, a discussion on the limitations of MD simulations, and an outlook for future work are presented in Chapter 7.

The three appendices contain non-crucial information for the results, but should give the reader the information needed to replicate our experiments, if so desired.

Introduction to Silicon Carbide

2.1 Properties of SiC

Silicon carbide (SiC) is a semiconductor compound consisting of the group IV elements silicon (Si) and carbon (C). Though SiC has been known as a semiconductor material since 1907, it was first widely known for its extreme hardness and its high thermal and chemical stability. With these properties, SiC has found many uses, for example as crucibles for melting metals, as a substitute for diamond in diamond-cutting tools, and even for producing car brakes and bullet-proof wests.[9, pp 6][10][11]

SiC became interesting as a semiconductor material, when researchers in the late 1950's found methods for growing large single polytype crystals.[9] The semiconducting properties of SiC are very different from Si (see table [2.1]), which is still the most used material in the semiconductor industry.

Though its carrier mobility is lower than that of Si, SiC has other properties that make it a good material for highly specialized devices: SiC has a high breakdown field, a large electron drift velocity, and a high thermal conductivity. Furthermore, due to its thermal stability it is able to operate at very high temperatures. Another great advantage of SiC is that its native oxide is SiO_2 which makes it highly compatible with Si based devices.[2]

Today, SiC is used for building high power devices and for devices which need to operate under extreme temperatures.[2]

SiC exists as several polytypes. These polytypes do not only have different crystal structures, their semiconductor properties, such as the electron band gap, vary greatly for each polytype, as seen table 2.1[9]. Researchers are now investigating which growth conditions favor which polytype and how to control the polytype formation. This is highly relevant since today's semiconductor device research is particularly focused on creating devices

	Si	3C SiC	4H SiC	6H SiC
Band gap at room temperature [eV]	1.1	2.3	3.2	3.0
Breakdown field [MV/cm]	0.6	>1.5	3	3.2
Saturated electron drift velocity [10^7cm/s]	1	2.5	2	2
Electron mobility [10^3cm^2/Vs]	1.1	0.75	0.80	0.37
Hole mobility [cm^2/Vs]	0.4	0.04	0.1	0.09
Thermal conductivity [W/cmK]	1.5	5.0	4.9	4.9
Maximum operating temperature [K]	600	1200	-	1580

Table 2.1: Electronic and thermal properties of SiC polytypes compared to Si. Table reproduced from [9, pp 8].

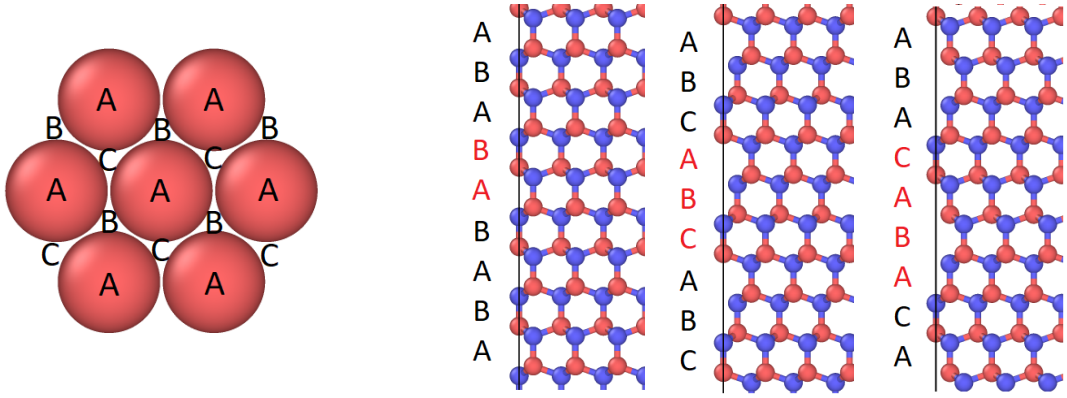

(a) Stacking pattern of (111)-surface. (b) 2H (c) 3C (d) 4H

Figure 2.1: The three polytypes of SiC tested in this report. The periodic sequence is marked in red.

with optimized electron band structures. If we gain control of the governing process of polytypism, we would be able to create a whole new series of electronic devices.

2.2 Polytypism of SiC

Polymorphism is the ability of certain materials to exist in different crystal structures. Polytypism is a special case of polymorphism where the structures only vary in one direction. When growing semiconductor nanowires, this direction is the growth direction; in this report the [111]-direction for cubic crystal structures or, equivalently, the [0001]-direction for hexagonal structures.

SiC nanowires are typically grown epitaxially, for example by the vapor-liquid-solid mechanism which is a layer-by-layer type of growth method.[2] Here, differences in the stacking sequence are what distinguish the polytypes from each other. Figure 2.1 illustrates how the difference in stacking sequence results in different crystal structures. In figure 2.1a we see the (111) surface of a SiC bi-layer which is situated at stacking sites A. The next bi-layer of atoms can either choose stacking sites B or C. Depending on the periodicity of how the bi-layers stack on top of each other, different polytypes are formed. In the figures 2.1b-2.1d the three polytypes used in this report are shown.

The polytypes are named using the Ramsdell notation[12]: "XN", where the number X is the number of bi-layers in the unit cell, and the letter N is either "C" for cubic structures or "H" for hexagonal structures.[9] The three polytypes are as follows: SiC (3C), SiC (2H), and SiC (4H). Each polytype is characterized by their stacking sequence and the hexagonality of their unit cells.

The unit cell of SiC (2H) has stacking sequence AB and is commonly known as Wurtzite (wz). The wz structure can be seen as two hcp lattices, one for Si-atoms and one for C-atoms, shifted by a fraction $\frac{3}{8}$ of the unit cell length, c, in the [0001]-direction. The SiC (2H) polytype has 100% hexagonality.

The unit cell of SiC (3C) has stacking sequence ABC and is commonly known as Zinc-blende (zb). Similarly to wz, the zb structure can be as two fcc lattices that are shifted with respect to each other by a fraction $\frac{1}{4}$ of a unit cell in the [111]-direction. The SiC (3C) polytype has 0% hexagonality.

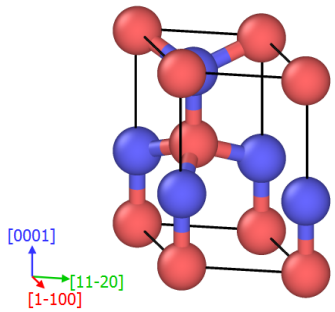

(a) Wurtzite (2H)

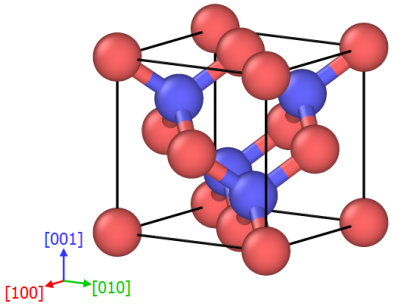

(b) Zinc-blende (3C)

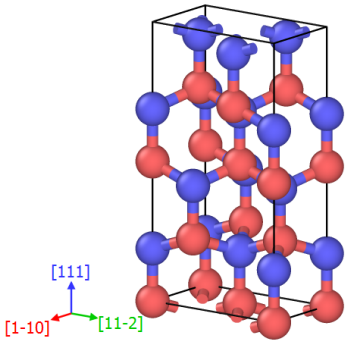

(c) 4H

Figure 2.2: Unit cells of the three polytypes tested in this report.

The unit cell of SiC (4H) has stacking sequence ABAC and has no commonly known name. It can be seen as an equal mixture of the (2H) and (3C) polytypes. It has a hexagonality of 50%.

The unit cells of the investigated three polytypes are shown in figure 2.2.

All the polytypes are found in SiC nanowires, albeit (2H) are rare.[6][7] However, we did not select these polytypes because they are common, but because they represent the range of hexagonality found in SiC polytypes. We choose polytypes of different hexagonality, because we assume the difference in crystal structure will cause differences in the mechanical properties.

Theory of Molecular Dynamics Simulations

3.1 Molecular Dynamics simulations

Molecular Dynamics (MD) simulations are a computational method of simulating the movement of each individual atom or molecule in a large system containing hundreds of thousands to several millions of atoms or molecules. MD simulations can be used to model systems in gaseous, liquid, and, as we will do in this report, solid phases.[4, p 5]

In a crystal solid, the atoms are hold together in the crystal lattice by the valence electrons forming bonds with the neighboring atoms. Electrons are inherently non-classical particles and the bonds formed by the valence electrons exhibit very complex quantum mechanical behavior which is hard to model accurately.[3, pp 237-238]

Using quantum mechanical modeling methods, such as density functional theory (DFT), researchers are able to accurately model small systems of maximum a thousand atoms for a timescale of up to 10 picoseconds with only few approximations.[3, table 5.2, p 281] But to model large systems of millions of atoms using quantum mechanical methods is simply not feasible with today's technology.

Instead, MD simulations treat the atoms as classical particles obeying Newtonian mechanics. The motion of each atom is found by solving Newtons second law of motion:

$$m_\alpha \vec{a}_\alpha = \vec{f_\alpha} \tag{3.1}$$

Here m_α is the mass of atom α, $\vec{a}_\alpha$ is the acceleration, and $\vec{f_\alpha}$ is the force acting on atom α. The force $\vec{f_\alpha}$ is given by the interaction potential V, which needs to be specified for the system:

$$\vec{f_\alpha} = -\vec{\nabla}_\alpha V(\vec{r}) \tag{3.2}$$

In general, the interaction potential consists of two parts: an external potential, V_{ext}, originating from external fields and constraints acting on the system, and an internal inter-atomic potential, V_{int}, which incorporates all the energy contributions arising from interactions between atoms and electrons inside the system.[3, p 492]

It is the inter-atomic potential, V_{int}, that has to replace the valence electrons role of forming bonds in the crystal structure. The justification for replacing the valence electrons with an effective potential is found in the Born-Oppenheimer approximation (BOA). In the BOA the movement of the electrons is assumed instantaneous on the timescale of the nucleus due to the large difference in mass. This means that at any time, for any configuration of the atoms in the system, the electrons can be assumed to have found their ground state characterized by the ground state energy E_g. A good inter-atomic potential,

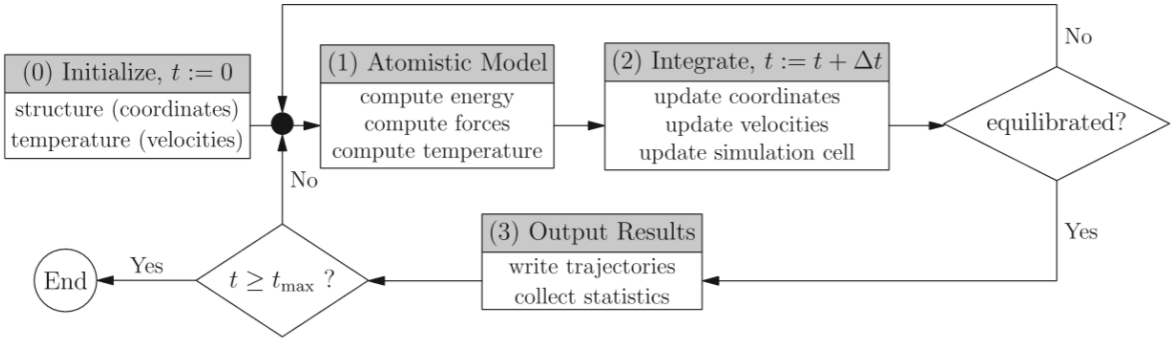

Figure 3.1: Flow chart showing the structure of a typical MD simulation. (*Reproduced from Modeling Materials by E. Tadmor and R. Miller[3, Fig 9.2 p 496]*)

V_{int}, is able to approximate the energy contribution of the elections as accurately as possible. [3, p 241]

In this report, we will use three different inter-atomic potentials and compare how they predict the mechanical properties and the fracture behavior of SiC nanowires. As the results will show, the different potentials produce different outcomes.

The steps of a MD simulation are graphically depicted in figure 3.1, which we reproduce from: [3, p 496]. The steps are as follows:

In the initialization step (0), the general system is set up, which includes specifying the initial dimensions of the system, the boundary conditions, the type of crystal structure, the type of atoms and their position in the unit cell. By specifying a temperature we can assign velocities to the atoms according to the temperature.

In step (1), the energy, forces, and temperature are computed according to the atomistic model chosen.

In step (2), the spatial coordinates and velocities of each atom are computed and updated via numeric integration of the equation of motion 3.1. The time increases by one time step. Choosing the right size of the time step is crucial for MD simulations. Essentially, the time step decides the resolution of the simulation. Small time steps give a high resolution, but also make the simulation very time consuming. When modeling solids, the resolution needs to be high enough to capture the vibrational motion of the atom. That requires a time step of 1 femtosecond or smaller.[3, pp 504]

Before obtaining our data, we need to ensure that the system is in equilibrium. Therefore an equilibration step is included in the flow chart. The steps (1) to (2) are repeated until some specified equilibrium criterion has been fulfilled. Only then we proceed to step (3).

In step (3) we obtain our data and write it to an output file. It is often not needed to save the data of every time step, since the changes in the system will only vary a little between each time step. In order to avoid unnecessary large output files of hundreds of gigabytes, the data is sampled when a specified number of time steps have passed. The steps (1) to (3) are repeated until the time has reached the specified number of time steps ($t = t_{max}$).

Theory of Inter-atomic Models

In this section we will introduce the three inter-atomic models used in this report. The models can be divided into two groups, depending on how they evaluate the potential energy of the system. The two groups are called cluster potentials and cluster functionals.

4.1 Cluster potentials

It can be mathematically shown that the exact potential energy of a many-body system containing N atoms can be expressed as an N-term series in the following form:[3, p 247]

$$V = \phi_0 + \sum_{i=1}^{N} \phi_1(\mathbf{r}^i) + \frac{1}{2!} \sum_{\substack{i,j \\ i \neq j}}^{N} \phi_2(\mathbf{r}^i, \mathbf{r}^j) + \frac{1}{3!} \sum_{\substack{i,j,k \\ i \neq j \neq k}}^{N} \phi_3(\mathbf{r}^i, \mathbf{r}^j, \mathbf{r}^k) + ... \tag{4.1}$$

Here each function ϕ_n is an n-body potential depending on a cluster of n atoms, and $\mathbf{r}^i$ is the position of atom i with respect to an origin O. The functions ϕ_n are required to be symmetric with respect to any permutation of their arguments: $\phi_2(\mathbf{r}^i, \mathbf{r}^j) = \phi_2(\mathbf{r}^j, \mathbf{r}^i)$. Another requirement is that ϕ_n will approach zero whenever one of its atoms is moved to infinity, since the n-body cluster should represent the "add-on" energy of the system after all the interactions of a smaller cluster of n-1 atoms has been calculated.

The first term in the series, ϕ_0, is the reference energy of the system and is given by the sum of the energies of the individual atoms in isolation from each other.[3, p 249]

$$\phi_0 = \sum_{i=1}^{N} E_{free}(Z^i) \tag{4.2}$$

Here $E_{free}(Z)$ is the energy of an isolated atom of atomic number Z.

The second term,ϕ_1, is a one-body term which represents the energy related to the atom interacting with an external potential, V_{ext}, outside the system.

$$V_{ext} = \sum_{i=1}^{N} \phi_i(\mathbf{r}^i) \tag{4.3}$$

If we ignore the external potential for a moment, we can focus on the internal inter-atomic potential V_{int}. It has been proven that an inter-atomic potential must fulfill the requirement of translational, rotational and parity invariance. This is called the basic representation theorem, and the consequence of this is that internal potential energy can only be a function of relative inter-atomic distances r^{ij}.[3, pp 243-244]

Since SiC is a compound, the n-body potentials ϕ_n will depend on the type of atoms in the interaction. We remember this by explicitly writing the atoms into the subscript, e.g.: ϕ_{ij}.

Using this notation, we write the internal inter-atomic potential as:

$$V_{int} = \phi_0 + \frac{1}{2!}\sum_{\substack{i,j \\ i\neq j}}^{N} \phi_{ij}(r^{ij}) + \frac{1}{3!}\sum_{\substack{i,j,k \\ i\neq j\neq k}}^{N} \phi_{ijk}(r^{ij}, r^{ik}, r^{jk}) + ... \tag{4.4}$$

Inter-atomic models using this formalism are called cluster potentials.

Since N is an incredibly large number, the exact potential which is a series of N terms would be an impossible task to evaluate. Therefore, it is assumed that an approximate model can be created by terminating the series at a small, but sufficiently large order of n.

For covalent materials, such as SiC, the atomic bonds are highly directional and the angle between two bonds will have great influence on the energy of the system. In order to evaluate the angles, the cluster potential series needs to go to the order of $n = 3$ to include a three-body term, since three atoms are needed to describe the angle between atoms.

Including angles in the potential is not a violation of the basic representation theorem, since an angle, θ_{ijk}, between two bonds $i - j$ and $i - k$ can be expressed as a function of the inter-atomic distances r^{ij},r^{ik},r^{jk}:[3, p 250]

$$\cos\theta_{ijk} = \frac{(r_{ij})^2 + (r_{ik})^2 - (r_{jk})^2}{2r_{ij}r_{ik}} \tag{4.5}$$

4.1.1 The cut-off distance

As mentioned earlier, we require the potentials, ϕ_n to tend to zero when one of the atoms is moved to infinity. In practice it is often needed to have the ϕ_n's tend to zero after a finite "cut-off" distance, r_{cut}, in order to reduce the computational time.[3, pp 245-246] This truncation can be implemented in various ways. The Vashishta potential is designed to tend to zero when the inter-atomic distance approaches r_{cut}.[13] For the Tersoff and the MEAM potential a cut-off function, f_{cut} is used:[14][15]

$$f_{cut}(r^{ij}) = \begin{cases} 1 & \text{, if } r^{ij} \leq r_{cut} - \frac{\Delta r}{2} \\ f_c(r^{ij}) & \text{, if } r_{cut} - \frac{\Delta r}{2} < r^{ij} < r_{cut} + \frac{\Delta r}{2} \\ 0 & \text{, otherwise} \end{cases} \tag{4.6}$$

The cut-off function is designed so it tends to zero within a specified length scale of Δr. The exact formulations of the $f_c(r^{ij})$ are given in the sections explaining the Tersoff and MEAM potentials.

4.1.2 The Vashishta potential

The Vashishta potential is a cluster potential developed by P. Vashishta et al., and it has been used to model semiconductor materials, ceramics, and inorganic compounds.[16] Relevant for this report is the 2007 paper by P. Vashishta et al., where the potential is adapted to model SiC of both zinc-blende and wurtzite structures.[13] The potential used in this report is adapted from the 2007 paper.

The Vashishta potential is based upon the well-known Stillinger-Weber potential[4, p 1913] and combines repulsive, screened Coulombic, screened charge-dipole, and dispersion interactions with bond angle energy.[16][4, p 1954]

The Vashishta potential is very computationally demanding, so in order to reduce the computational time we choose a method which tabulates the analytical values of 100,000 points between a radius $R_{innercut} = 2.5\,\text{Å}$ to the cut-off radius $R_{cut} = 2.9\,\text{Å}$. This increases the speed with very little loss of accuracy.[4, p 1955]

In the Vashishta potential, the interaction energy is given by the sum of a two-body and a three-body term:

$$V_{int} = \sum_{i}^{N}\sum_{j>i}^{N} \phi_{ij}\left(r_{ij}\right) + \sum_{i}^{N}\sum_{j\neq i}^{N}\sum_{k>j,k\neq i}^{N} \phi_{ijk}\left(r_{ij}, r_{ik}, \theta_{ijk}\right) \tag{4.7}$$

The two body term is given by:

$$\phi_{ij}(r) = \frac{H_{ij}}{r^{\eta_{ij}}} + \frac{Z_i Z_j}{r}\exp\left(-r/\lambda_{1,ij}\right) - \frac{D_{ij}}{r^4}\exp\left(-r/\lambda_{4,ij}\right) - \frac{W_{ij}}{r^6}, r < r_{c,ij} \tag{4.8}$$

The three body term depends on the bond angle θ_{ijk} relative to the reference bond angle θ_{0ijk}, and is given by:

$$\begin{aligned}\phi_{ijk}\left(r_{ij}, r_{ik}, \theta_{ijk}\right) =& B_{ijk}\frac{\left[\cos\theta_{ijk} - \cos\theta_{0ijk}\right]^2}{1 + C_{ijk}\left[\cos\theta_{ijk} - \cos\theta_{0ijk}\right]^2}\times \\ & \exp\left(\frac{\gamma_{ij}}{r_{ij} - r_{0,ij}}\right)\exp\left(\frac{\gamma_{ik}}{r_{ik} - r_{0,ik}}\right), r_{ij} < r_{0,ij}, r_{ik} < r_{0,ik}\end{aligned} \tag{4.9}$$

The values and meaning of the fitting parameters: H_{ij}, η, Z_i, Z_j, λ_1, λ_4, r_c, r_0, γ, D_{ij}, W_{ij}, B_{ijk}, C_{ijk}, $\cos(\theta_{0ijk})$ are given in appendix B.1.

4.2 Cluster functionals

In the previous section we described cluster potentials in which the inter-atomic potential is constructed as a series of n-body terms. It was assumed that the interaction could be accurately approximated by terminating the series at a small, but sufficiently high order of n. However, for some materials this conversion is slow, and higher order n-body terms must be included. This increases the computational time dramatically.[3, pp 267-268]

To overcome this, cluster functionals were developed. A cluster functional consists of a simple pair potential term, as well as a functional term which represents the electron environment of the atom. The functional is designed to replace the high order n-terms and thereby save computational time. Cluster functionals also have the advantage that the formulation is more general than cluster potentials and therefore are able to model a broader range of atomic configurations[3, p 283], as will be discussed in section 7.2.

In order to model covalently bonded materials, the functional needs to incorporate a three-body term. This allows for taking into account the directionality of the covalent bonds, as described earlier.

In this report we will use two well-known cluster functionals: the Tersoff potential and the MEAM potential.

4.2.1 The Tersoff potential

The Tersoff potential is a cluster functional developed by J. Tersoff in the years 1986 to 1989.[3, p 269] Originally designed to model the covalent bonding of Si[14], J. Tersoff

expanded the model in 1989 to incorporate compounds like SiC.[17] The model of the 1989 paper by Tersoff is used in this report.

In the Tersoff potential, the inter-atomic potential is given by:

$$V^{int} = \frac{1}{2} \sum_{\substack{i,j \\ i \neq j}} f_c(r^{ij}) \left[\phi_R(r^{ij}) + b(z^{ij}) \phi_A(r^{ij}) \right] \tag{4.10}$$

Here f_c is a cut-off function, which will be explained below, ϕ_A and ϕ_R are two pair potentials modeling attractive and repulsive interactions respectively. They are given by:

$$\phi_R(r^{ij}) = A \exp^{-\lambda_1 r^{ij}} \tag{4.11}$$

$$\phi_A(r^{ij}) = -B \exp^{-\lambda_2 r^{ij}} \tag{4.12}$$

Here A, B, λ_1, and λ_2 are fitting parameters, and r^{ij} is the distance between atom i and atom j. The attractive pair potential is modified by the three-body functional term $b(z)$:

$$b(z^{ij}) = (1 + (\delta^{ij} z^{ij})^n)^{-1/2n} \tag{4.13}$$

Here δ^{ij} and n are fitting parameters. The coordinate function z^{ij} is given by:

$$z^{ij} = \sum_{\substack{k \\ k \neq (i,j)}} f_c(r^{ik}) g(\theta^{ijk}) \exp^{\lambda_3^3 (r^{ij} - r^{ik})^3} \tag{4.14}$$

The coordinate function depend on the bond angle θ^{ijk}, which is quantified through the function g:

$$g(\theta^{ijk}) = 1 + \frac{c^2}{d^2} - \frac{c^2}{d^2 + (\cos(\theta^{0ijk}) - \cos(\theta^{ijk}))^2} \tag{4.15}$$

Here c and d are fitting parameters, and $\cos(\theta^{0ijk})$ is the optimal bond angle.

The cut-off function,f_c, is given by:

$$f_c(r^{ij}) = \begin{cases} 1 & \text{, if } r^{ij} < R - D \\ \frac{1}{2} - \frac{1}{2} \sin(\frac{\pi}{2} \frac{r^{ij} - R}{D}) & \text{, if } R - D \leq r^{ij} \leq R + D \\ 0 & \text{, if } r^{ij} > R + D \end{cases} \tag{4.16}$$

Here the cut-off parameters R and D determine the region in which the cut-off function approaches zero.

In total the Tersoff potential has twelve fitting parameters: A,B,λ_1,λ_2,λ_3,δ,n,R,D,c,d and $\cos(\theta^{0ijk})$. All the parameters are given in the appendix B.2.

4.2.2 The MEAM potential

The Modified Embedded Atom Method (MEAM) potential was developed by Basker et al. in the years 1989 to 1992. The MEAM potential is a modified version of the EAM potential, which is commonly used to model metals[4, pp 1677]. In both potentials the energy is given by a pair potential term, ϕ_{ij}, and an embedding energy functional term F_i,

which represents the energy of embedding the atom in an environment of electron density $\overline{\rho}_i$:

$$E = \sum_i \left[F_i\left(\overline{\rho}_i\right) + \frac{1}{2} \sum_{j(\neq i)} \phi_{ij}\left(r_{ij}\right) \right] \tag{4.17}$$

The modification of the MEAM potential with respect to the EAM potential comes from the way the electron density is calculated; instead of just having the spherically-averaged zeroth order term $\overline{\rho}_i^{(0)}$, the MEAM potential adds three additional terms: $\overline{\rho}_i^{(1)}$,$\overline{\rho}_i^{(2)}$, and $\overline{\rho}_i^{(3)}$. These terms are included in order to simulate the directional dependence of the electron density.[3, p 277] The MEAM potential is therefore used to model materials with highly directional bonding, such as covalent materials[4, p 1793].

We implement the formalism described by Gullet et al.[15]. The complete formalism of the MEAM potential is rather lengthy, therefore we move it to appendix A.

The cut-off function is given by:

$$f_{cut}(x) = \begin{cases} 1 & x \geq 1 \\ \left[1 - (1-x)^4\right]^2 & 0 < x < 1 \\ 0 & x \leq 0 \end{cases} \tag{4.18}$$

Where x is equal to: $x = \frac{r_{cut} - r_{ij}}{\Delta r}$

Method

5.1 List of softwares

To perform the MD simulation, we use the software LAMMPS. The name is an acronym and stands for "Large-scale Atomic/Molecular Massively Parallel Simulator". It is an open-source code developed by Sandia National Laboratories designed to perform molecular dynamics simulations with special focus on material modeling.[4]

To operate LAMMPS, an input file is created with all the commands LAMMPS needs to execute. In the next section, we will show excerpts of such an input file and explain the commands essential for our studies.

LAMMPS has a built-in library of inter-atomic models with fitting parameters for a list of selected materials. The potentials for SiC used in this report are all found in the LAMMPS library.

The output file of LAMMPS is a long .txt file containing the x, y, and z-coordinates, the potential energies, and the stress for each atom at each time step. To visualize all this data, we use the open-source program Ovito.[18] Using this software allows us to investigate the output data in various ways: we can examine the nanowires at every time step to visually determine the fracture behavior, we can also assign colors to each atom depending on their potential energy or the stress acting on it, and thereby form 3 dimensional maps of the potential energy and stress distribution in the structure. Ovito also includes a dislocation analyzer tool, called DXA, which we will use for the dislocation analysis.[19]

For plotting, fitting, and various computations we use the program Matlab 2016b, which is a commonly used software in academia.[20]

5.2 Excerpts of an input file

To run LAMMPS, an input file needs to be created. In the appendix C, an example of the full input file is shown. In the following section, we will restrict ourselves and only explain the most crucial parts of the input file. Please note that lines starting with a "#" are not read by LAMMPS and are intended to make the file more easily interpreted by the reader.

The input file starts by defining the units of the system, the dimensionality (3D), and the boundary conditions, as shown in the box below. We choose periodic boundary conditions in all three directions. This will allow us to perform the isobaric relaxation later on.

```
units metal
dimension 3
```

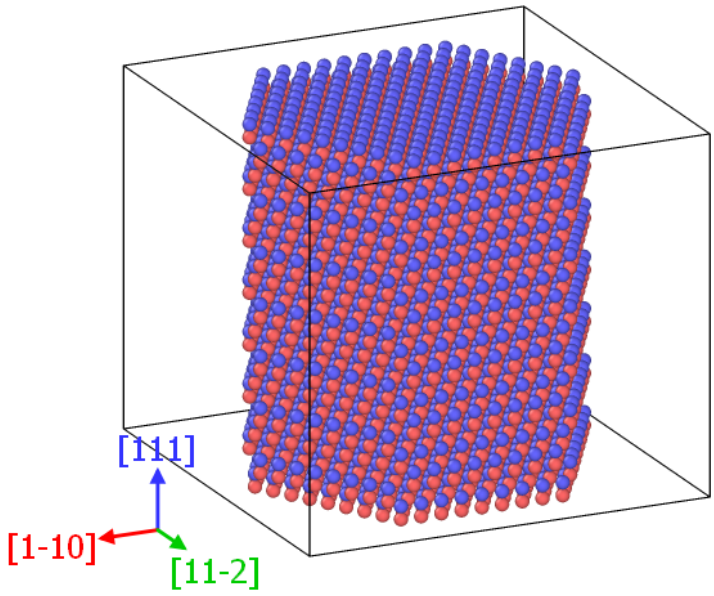

Figure 5.1: The system simulated. The edges of the simulation box are marked with black lines. Inside is a SiC (3C) nanowire. Red atoms are Si and blue atoms are C.

```
boundary p p p
atom_style atomic
```

Next we create the simulation box. The box defines the size of our system, and its surfaces are the periodic boundaries of the system. The length scale of the box is the lattice parameter `latconst_a`, which is the length size of the polytype unit cell.

```
#---Create simulation box---
lattice fcc ${latconst_a}
region simbox block -5 5 -5 5 -0.01 ${height}
create_box 2 simbox
```

In the following section, we create the nanowire by merging four prisms of equal heights and lengths but with different orientation. This creates the hexagonal cross section of the nanowire. The height of the nanowire is the same as the simulation box, while the diameter of the nanowire is two unit cells smaller than the width of the simulation box. This ensures there is no interaction across the periodic boundaries in the xy-plane while having interaction across the boundaries in the z-direction. What we create is a nanowire which can be seen as a small section of an infinitely tall, free standing nanowire.

When we later on simulate bulk SiC, we will not create this nanowire region, but have the crystal lattice fill the entire simulation box.

```
#---Defining nanowire ---
region nprism1 &
prism 0 ${rad_p} -0.01 ${SiC_yp} -0.01 ${height} ${SiC_xn} 0 0
region nprism2 &
prism ${rad_n} 0 -0.01 ${SiC_yp} -0.01 ${height} ${SiC_xp} 0 0
region nprism3 &
prism ${SiC_xn} ${SiC_xp} ${SiC_yn} -0.01 -0.01 ${height} ${SiC_xn} 0 0
```

```
region nprism4 &
prism ${SiC_xn} ${SiC_xp} ${SiC_yn} -0.01 -0.01 ${height} ${SiC_xp} 0 0

region         nanowire union 4 nprism1 nprism2 nprism3 nprism4
```

In the section below, we create the Zinc-blende unit cell found in SiC (3C) polytypes. The z-axis is aligned with the [111] crystal orientation. The x- and y-axis alignment shown below will create a nanowire with surfaces of type {1-10}. Surfaces of type {11-2} can also be created by rotating the crystal lattice 30° around the z-axis.

We add atoms of type 1 and 2 to the basis of the unit cell and map the Zinc-blende crystal lattice to the region defined `nanowire`.

```
#---Creating the zb lattice (normalized z[111]-direction)
lattice        custom ${latconst_a} &
orient x 1 1 -2 orient y -1 1 0 orient z 1 1 1 &
a1 1.0 0.0 0.0 &
a2 0.0 1.0 0.0 &
a3 0.0 0.0 1.0 &
basis 0.0 0.0 0.0        basis 0.0 0.5 0.5 &
basis 0.5 0.0 0.5        basis 0.5 0.5 0.0 &
basis 0.25 0.25 0.25        basis 0.25 0.75 0.75 &
basis 0.75 0.25 0.75        basis 0.75 0.75 0.25

#---Adding atoms---
create_atoms 2 region nanowire &
basis 1 1 basis 2 1 basis 3 1 basis 4 1 &
basis 5 2 basis 6 2 basis 7 2 basis 7 2

group nanowire region nanowire
```

Next we define the atom types and mass, and choose the inter-atomic potential. In this case the MEAM potential:

```
#---Defining Atomic potential---
mass        1 28.085
mass        2 12.011
group Si type 1
group C  type 2

pair_style        meam/c
pair_coeff        * * library.meam Si C SiC.meam Si C
```

A random number generator assigns velocities to the atoms in the system by sampling an uniform distribution, which are scaled to match the specified temperature, here: 0.01 Kelvin. The generator uses the same seed of generation (511124) for every simulation, which allows for reproducible simulations. The total linear and angular momenta of the generated ensemble of velocities are set to zero:

```
#---Initial velocities
velocity        all create 0.01 511124 rot yes mom yes
```

Before obtaining any data, we have an equilibration step where we minimize the energy of the system. The command `box/relax iso 0.0` allows for changing the size and form of the simulation box during the minimization while keeping a constant isobaric pressure of 0.0 bar.

The style of minimization is the steepest descent method, and we minimize the structure for 50000 time steps or until the change in potential energy is below the stopping tolerance of 10^{-25} eV.

We choose a rather small time step of 0.1 femtosecond, since the equilibration is a "fine-tuning" step.

```
#---Bar stat---
timestep   0.0001
fix         RELAXBOX all box/relax iso 0.0
min_style sd
minimize 1e-25 1e-25 50000 100000
unfix RELAXBOX
```

In the following step, we start the MD simulation. We choose an NVT type of integration where the number of particles, volume of simulation box, and temperature are kept constant during the integration step.

The mechanical properties of the SiC samples are obtained through tensile testing, which is done by expanding the simulation box in the z[111] direction at an engineering strain rate of $\dot{\epsilon} = 10^8\,\mathrm{s}^{-1}$. The strain rate in MD simulations is many orders of magnitude higher than the strain rates used in real life tensile testing experiments. The high strain rate is not desired, but is a consequence of the timescales (of order picoseconds) used in MD simulations. We choose a strain rate of $10^8\,s^{-1}$ because it is the standard used in many MD simulation tests.

We choose a time step of 1 femtosecond, which is a standard time step for modeling solids.[3, p 504] We perform 3 million iterations to reach a final strain of 30%.

```
#---Timeintegration---
fix        NVT all nvt temp 0.01 0.01 0.1

#----Start loading, strain rate 1e8 (1e-4)---
fix        LOAD nanowire deform 1 z erate 0.0001 units box

#----MD run (Loading)-------
timestep   0.001
run        3000000
```

Results

6.1 Comparison of inter-atomic potentials

Before we start our study of the SiC polytypes, we want to compare the three inter-atomic potentials: the Vashishta, the Tersoff and the MEAM potential, to see how they predict the mechanical properties and fracture behavior of SiC. We test the potentials for the same two structures: a nanowire of diameter 30.8 Å and a bulk structure of dimensions 4x4x6 unit cells (with periodic boundary conditions). The temperature is set to 0.01 Kelvin and the polytype tested is SiC (3C).

The mechanical properties we choose to compare are: the Young's modulus, the maximum stress before failure, and the fracture strain which is the strain right before the fracturing. Using the software Ovito, we investigate the fracture behavior of the nanowires.

Influence of the cut-off function f_{cut}

All the inter-atomic potentials we test use cut-off methods to lower the computational time, however for the Tersoff potential we find that the cut-off function will influence the result of the tensile testing.

In the original 1989 paper by J. Tersoff, the cut-off parameters are: $R = 2.36\,\text{Å}$ and $D = 0.15\,\text{Å}$. These values are not systematically optimized, but are chosen to include the interaction for first nearest neighbors only.[17] The short range of the potential reduces the computational time needed.

However, in our report the original parameters for the cut-off function turn out to be problematic. When the material is strained due to the mechanical loading, the inter-atomic distance between the first nearest neighbors will eventually reach the cut-off region that starts at: $R - D = 2.21\,\text{Å}$. When two atoms interact within the cut-off region, the energy of the bond pair is no longer given by the physically based potential but by the arbitrarily chosen cut-off function. This leads to an error in the calculated energy and results in a stress-strain curve that greatly differs from the expected. This can be seen in figure 6.1b (blue curve). This unwanted influence of the cut-off functions has also been documented by others and is attributed to a discontinuity of the second derivative of the cut-off function.[21]

Moving the cut-off region further away by increasing the size of R will solve this, but we have to be careful when choosing the new cut-off parameters. If we choose an R and D which place the cut-off region at distances near the third nearest neighbor, we would have the same problem of interaction in the cut-off region, albeit with a smaller error in the calculated energy, since the Tersoff potential approaches zero for large distances. The distance between third nearest neighbors is 3.61 Å for SiC (3C), indicated by the third arrow in figure 6.1a.

Instead we choose cut-off parameters: $R = 3.10\,\text{Å}$ and $D = 0.15\,\text{Å}$, which moves the

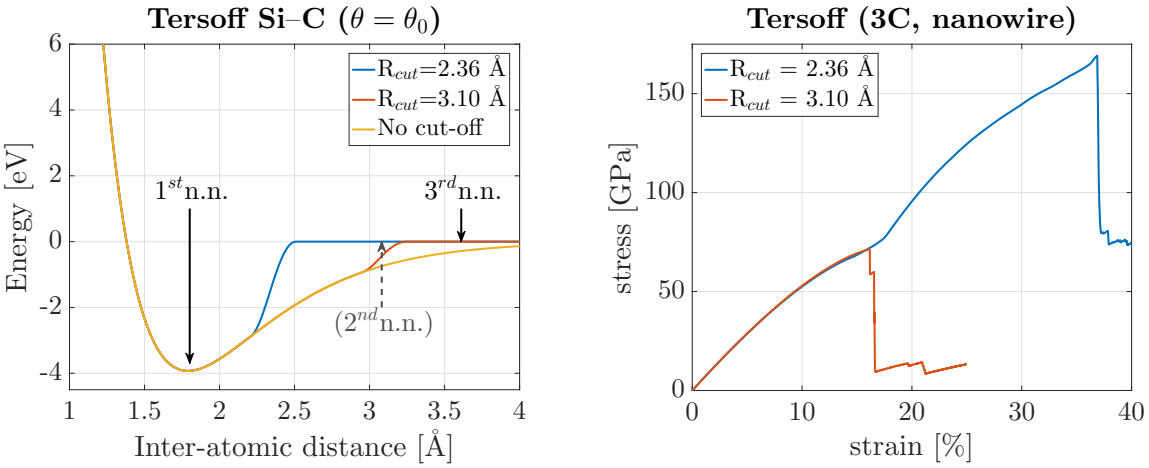

(a) Tersoff potential

(b) Tensile test

Figure 6.1: Part a) shows the Tersoff potential for Si - C interactions with the original cut-off parameters and our choice of the cut-off parameters. Part b) shows a tensile test performed on two identical nanowires using the potentials shown in a).

cut-off region in between the first and third nearest neighbors. The distance to the second nearest neighbor does not matter, since these atoms are of the same kind and therefore interact using a far smaller value of $R = 2.86\,\text{Å}$ (see appendix B.2). This allows the material to expand until failure without interaction in the cut-off region (see figure 6.1b, orange curve). Of course not having the cut-off function at all would be preferable, but it is not possible since the computational time would be immense.

The cut-off radii of the Vashishta and the MEAM potential are: 7.35 Å and 4.00 Å. These potentials do not show any issues regarding the cut-off function.

Mechanical properties

In figure 6.2 we see that the three potentials produce different results. The results of the testing are summarized in table 6.1. The Young's modulus is found by making a linear fit in the region 0-1% strain, the uncertainty of the fitting parameter is given in table 6.1. The maximum stress and fracture strain is read off the graph as indicated by the arrows in figure 6.2.

The Vashishta potential gives the lowest fracture strain of the three potentials: 10.1% strain for the nanowire and 14.4% for the bulk structure. It also produces the lowest Young's modulus and maximum stress. The Tersoff potential has an intermediate fracture strain of the three potentials: 16.2% for the nanowire and 21.6% for bulk. It produces the highest Young's modulus, but only the second highest maximum stress due to it fracturing earlier than the MEAM potential, which fractures at 25.3% for the nanowire and 28.7% for the bulk.

The bulk samples have higher Young's modulus than the nanowires. This is due to a higher material stiffness. The free surfaces of the nanowires are less stiff than the bulk due to the missing neighbors which allow the surface atoms to move more freely. This lowers the overall stiffness in the nanowires and results in lower values for the Young's modulus.

The nanowires consistently show lower fracture strain than the bulk samples. This is due to the surface atoms having higher potential energies than the bulk atoms (which will

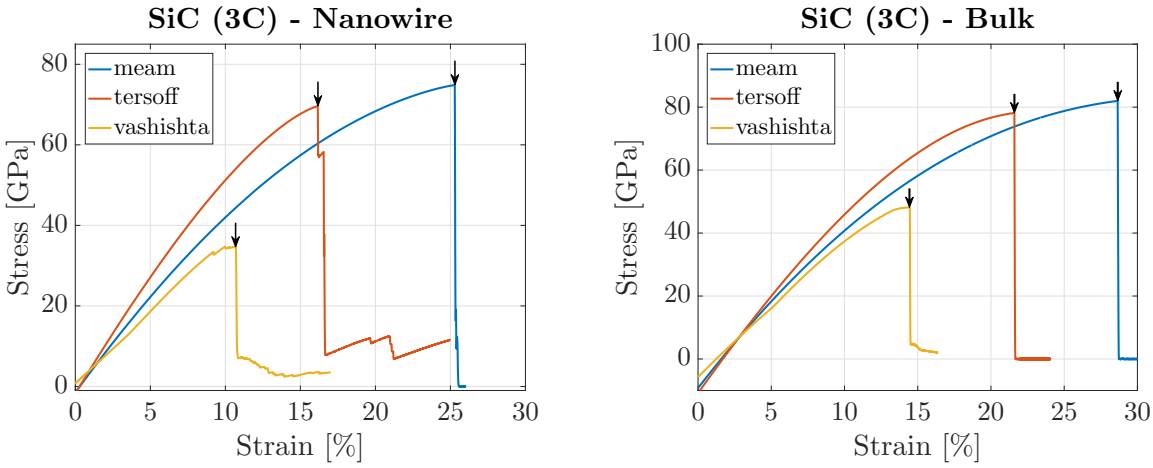

(a) (b)

Figure 6.2: Stress-strain curves for bulk and nanowire samples modeled by the three inter-atomic potentials.

Polytype	Potential	Bulk/ Nanowire	Young's modulus [GPa]	Tensile Strength [GPa]	Fracture Strain [%]
3C	MEAM	Bulk	589 ± 0.3	91.1	28.7
		Nanowire (30.8 Å)	502.4 ± 0.4	74.8	25.3
	Tersoff	Bulk	646.8 ± 0.2	88.9	21.6
		Nanowire (30.8 Å)	604.7 ± 0.2	69.6	16.2
	Vashishta	Bulk	461.1 ± 0.1	53.7	14.4
		Nanowire (30.8 Å)	342 ± 0.7	34.7	10.1

Table 6.1: Table of mechanical properties of identical structures modeled using three different inter-atomic potentials. The nanowires have diameter 30.8 Å and side facet of the surface type {11-2}.

be shown in section 6.2). Therefore the surfaces function as a catalyst for fracturing.

To evaluate the potentials, we compare with the results of MD simulations of SiC (3C) found in the literature. However, only a few papers with adequate comparisons could be found. Those are listed in table 6.2. The Tersoff potential was used in all the papers.

The results obtained in the papers vary, but are within the range of our own results. The paper that is most comparable with our experiment is the paper by M. A. Makeev et. al. [22]. Here they simulate nanowires of hexagonal cross-section at 0.1 Kelvin with mechanical loading along the [111] crystal direction. They find a Young's modulus that is closest to the result obtained by the MEAM potential in our experiment.

Fracture behavior

While the shapes of stress-strain curves for the three potentials look similar in the bulk samples (figure 6.2b), the curves show very different behavior after the initial fracture for the nanowire samples (figure 6.2a). To explain this, we need to look at the fracture behavior of the nanowires.

Figure 6.3 shows the structures immediately after the fracture for both the bulk and

Structure	Loading direction	Strain rate [s^{-1}]	Temperature [Kelvin]	Young's modulus [GPa]	Max tensile stress [GPa]	Fracture strain [%]	ref.
block 22x22x70 [Å]	[001]	3e10	10	440	86	32.5	[23]
cylinder 25-50 Å (diameter)	[110]	1e10	300	442	88.8	34	[24]
nanowire 89Å-356Å (diameter)	[111]	-	0.1	520.2-537.4	-	-	[22]
bulk	[100]	1e8	300	495.7	78.1	32	[25]

Table 6.2: Values for the MD simulations of SiC (3C) found in selected literature. The Tersoff potential was used in all cases.

the nanowire samples. For the bulk samples, the fractures behave similarly for all three potentials. This falls in line with the similar shaped stress-strain curves in figure 6.2.

For the nanowires, however, the Vashishta and Tersoff potentials produce quite different results compared to the MEAM potential. All the potentials show mode I fractures: the fracture develops at the surface where the potential energy is higher (as will be proven in the following section) and the planes of the fractured surfaces are normal to the loading direction.

However, in the cases of the Vashishta and Tersoff potentials, the nanowire does not fracture at once. Instead, on the three silicon rich surfaces of hexagon cross-section, the surface atoms form "bridges" which connect the two parts of the nanowire. This is most clearly seen in the case of the Tersoff potential (figure 6.3). When the structures are strained further, these bridges will stretch and hold the two pieces of the fractured nanowire together. This is why the stress-curves in figure 6.2a never go to zero but stay at a small positive value for the cases of the Vashishta and Tersoff potential.

Since the Si atoms have lower potential energy than the C atoms (see section 6.2), it makes sense if the Si rich surfaces break less easily than the C rich surfaces. However, the formation of "bridges" is not explained and no previous examples of this was found in the literature. The MEAM potential does not form any bridges, but we do see clear displacements of the Si-atoms on the Si rich surfaces (see figure 6.3 (f)).

Since the potentials do not show this behavior in the bulk cases, it must be a surface effect of the nanowires.

For the next series of simulations, we will continue using just one of the three potentials. The MEAM potential shows the most predictable behavior: the stress-strain curve is shaped as how we would expect for a brittle material, the mechanical properties are similar to what is found in literature (see table 6.2), and the fracturing is a mode I fracture with no unexplained surface effects. The Tersoff potential is the most used potential in the literature, but since its behavior is sensitive to the choice of cut-off parameters (see figure 6.1) and due to the unexplained surface effects during the fracture, we refrain from using it. The Vashishta potential was not chosen either, because it produces mechanical properties which are lower than what is found in the literature and also shows the unexplained fracture behavior. Therefore we choose the MEAM potential for our further studies.

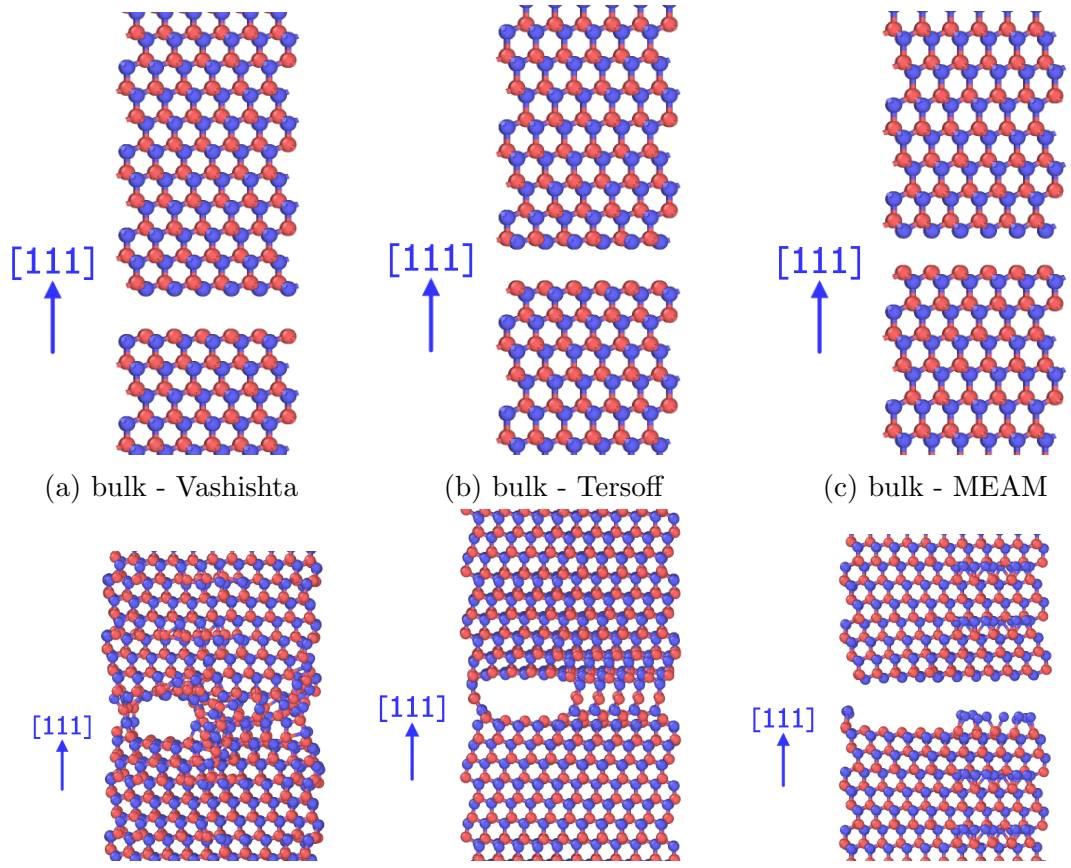

(a) bulk - Vashishta (b) bulk - Tersoff (c) bulk - MEAM

(d) nanowire - Vashishta (e) nanowire - Tersoff (f) nanowire - MEAM

Figure 6.3: Fracturing of bulk and nanowire SiC (3C) samples using the three different inter-atomic potentials. Nanowires are shown with the [1-10] direction pointing out of the page, meaning that two different surfaces are shown: the C rich on the left and the Si rich on the right (this is not obvious from the pictures).

6.2 Crystal surfaces

The nanowires tested in this report are oriented with the growth direction [111] along the z-axis, for which we will use notation: z[111]. A hexagonal cross section of the nanowire can be created in two ways: either by aligning the ⟨1-10⟩ or the ⟨11-2⟩ crystal directions along the diagonals of the hexagon. With the notation "$\langle \cdots \rangle$" we mean any direction of this family which *also* is orthogonal to the growth direction z[111].

The two orientations differ by a 30° rotation about the z[111] axis. The first orientation results in side facets of the type {11-2}, seen in figure 6.4a and 6.4c. The second orientation results in side facets of the type {1-10}, seen in figure 6.4b and 6.4d.

These two types of surfaces are known to have different chemical properties, for example the {11-2} surfaces are slightly polar, meaning that three of the surfaces have a higher ratio of Si to C atoms than the other three. The {1-10}-surfaces do not have this polarity.

Using MD simulations, we want to test if the two surface types will effect the mechanical properties of a nanowire of the same dimensions. We also want to compare the surface energy of the two surface types.

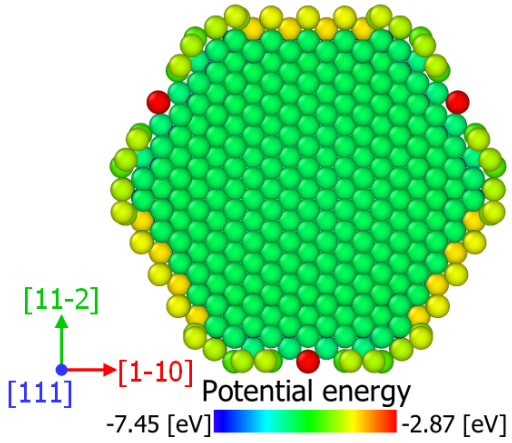

(a) {11-2}: top view

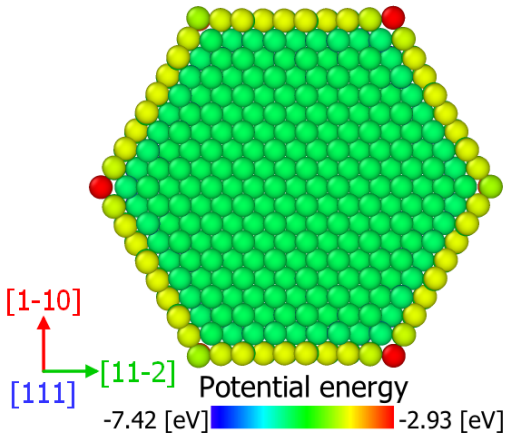

(b) {1-10}: top view

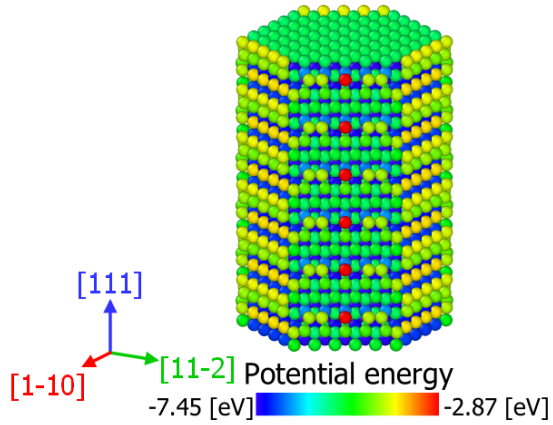

(c) {11-2}: 3D view

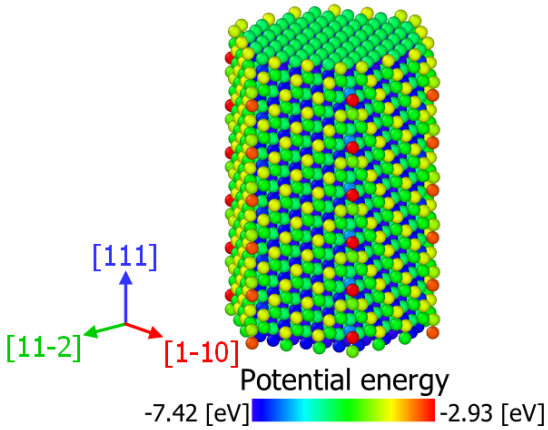

(d) {1-10}: 3D view

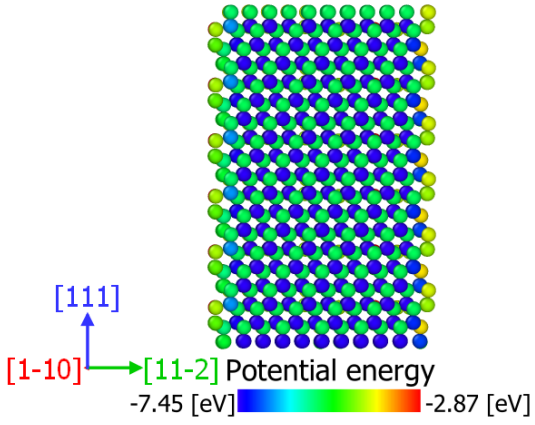

(e) {11-2}: Cut-through

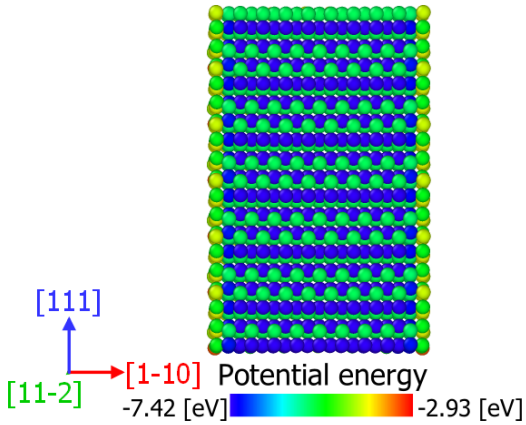

(f) {1-10}: Cut-through

Figure 6.4: Map of potential energy per atom as coloring. The structures are SiC (3C) with {11-2} surfaces (left) and {1-10} surfaces (right). Please note the orientation varies on each image.

Surface energy

Before comparing the surface energy of the two surface types, we ensure that the structures are in their thermodynamic equilibrium by minimizing the potential energy using the minimization method described in the method section. Figure 6.4 shows the potential energy of the two structures after minimization. By comparing figures 6.4c and 6.4d, we immediately see the structural difference of the two surface types. The polarity of the {11-2} surface can also be seen; due to different atomic numbers, the C atoms have a higher potential energy, and in the figure they appear more yellow than the Si atoms.

The bright red atoms, which can be seen on both structures, are Si atoms situated at stacking site C in the ABC stacking sequence. On the {11-2} facets these atoms displace in order to minimize the potential energy, and the center atom is left without a partner. On the {1-10} facets the red atoms are situated at the corners of the hexagon shape. Due to their positions these atoms protrude the most from the surface and therefore have the highest potential energy.

For both structures, we see that the surface atoms have higher energies than their bulk counterparts. This is a known effect and is due to the missing neighbors of the surface atoms. The unpaired electrons, in some literature called "dangling bonds", will increase the energy of the surface atoms compared to the bulk atoms.

In table 6.3, we show the average potential energy per atoms for both surface atoms and bulk. We define the surface atom as the outermost complete layer of atoms. In figures 6.4a and 6.4b, the surface atoms are seen as those of different color than their bulk counterpart. We estimate the surface energy as the difference between the average potential energy of surface and bulk atoms. When assuming a surface thickness of 1 Å, we find the surface energy per area: γ. These surface energies are listed in table 6.3. In the paper by E. Abavare et al.[26] the surface energy of SiC (3C) (111) surfaces was estimated using DFT and found to be in the range: 2446-2856erg/cm^2 depending on the method of calculation. The estimates used in our method are very close to these values.

Surface type	Average E_{pot} per surface atom [eV/atom]	Average E_{pot} per bulk atom [eV/atom]	Surface energy [eV/atom]	γ [erg/cm^2]
{11-2}	-4.72	-6.43	1.71	2630
{1-10}	-4.58	-6.43	1.85	2720

Table 6.3: Potential and surface energy of the two surface types.

Mechanical properties

To investigate how the surface type affects the mechanical properties, we perform tensile testing similarly to the section above. Figure 6.5 shows how the relative stress is distributed in the two structures at a strain of 15%. LAMMPS is able to compute the stress on each atom in the structure. However, since the volume of an atom is not well defined in MD simulations (assumed to be point particles), we cannot give a precise value of the stress on each individual atom, only on the structure as a whole, which has a well defined volume. That is why figure 6.5 shows the relative stress and not the actual stress.

By comparison, we see that structures with {1-10} surfaces distribute the stress more equally between surface and bulk atoms compared to the structure with {11-2} surfaces.

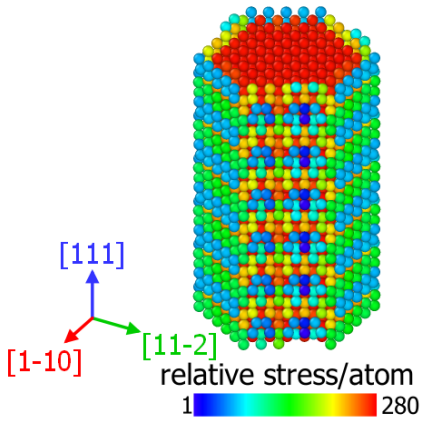

(a) {11-2}

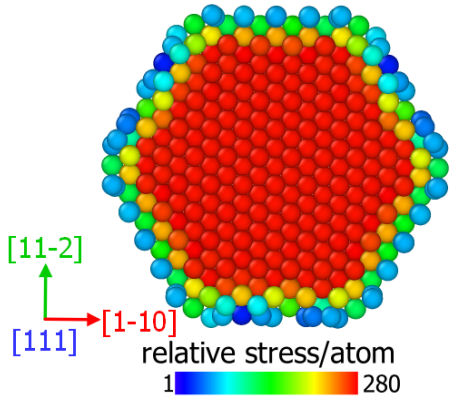

(b) {11-2}

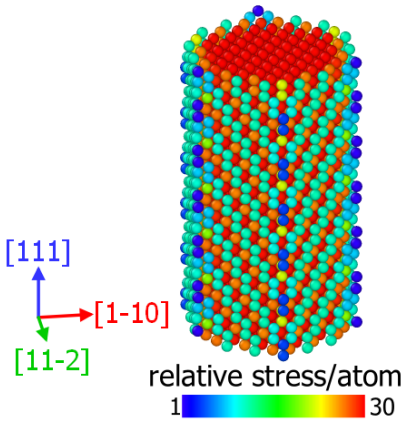

(c) {1-10}

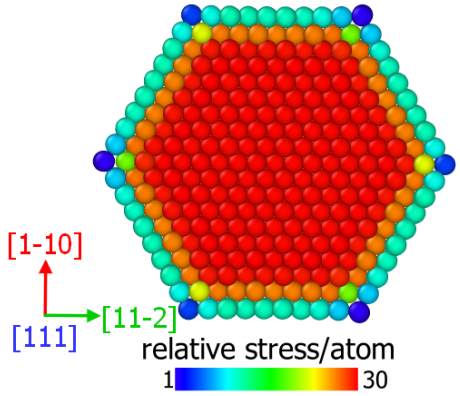

(d) {1-10}

Figure 6.5: Stress distribution at 15% applied strain for SiC (3C) nanowires of surface type {11-2} and {1-10}.

The difference in stress is due to the different stiffness in the structure. The higher the stiffness, the higher the stress under the same applied strain. Due to the missing neighbors, the surface atoms can move more freely and are therefore less stiff than the bulk. From figure 6.5 we learn that surfaces of type {1-10} have higher stiffness than {11-2}surfaces.

Figure 6.6 shows the stress-strain curves of the tensile testing. We see that surfaces of type {11-2} give rise to higher Young's modulus and maximum tensile strength, but lower fracture strain compared to surfaces of type {-110}.

We hypothesize that the lower fraction strain might be due to the surface structure. By comparing figure 6.4e with 6.4f, we see the difference in the structure of the surfaces. The {11-2} surfaces contain more dents and protrusions, which might serve as sites for which the fracture can develop, resulting in a lower fraction strain.

For the next series of tests, we will continue using nanowires with side facets of the surface type {11-2}. The reason being that it has the lowest surface energy and therefore it might be more likely to find in nature.

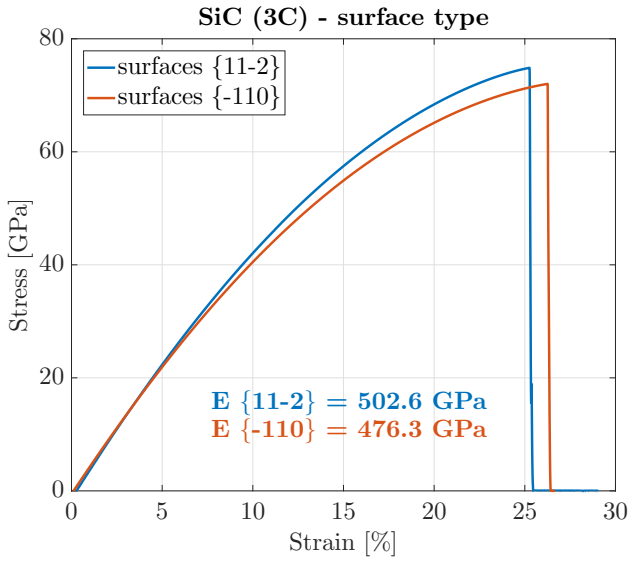

Figure 6.6: Stress-strain curves for SiC (3C) of the two surface types. The Young's modulus is shown in the graph.

6.3 SiC polytypes and temperature dependence

Next we create nanowires of similar dimensions with different polytypes: (2H), (3C), and (4H). We want the diameter of the nanowires to be a integer number of unit cells. Due to the size difference in the unit cells of the three polytypes, we cannot get the nanowire diameters to be the exact same (see 6.4). To minimize the difference we choose to create fairly wide nanowires of 50-52 Å diameters, resulting in a difference of 4%.

We find and compare the mechanical parameters of each polytype at four different temperatures. We will also investigate if there is any difference in the fracturing of the polytypes. Since SiC is a known brittle material, we expect to see brittle fractures. At high temperatures some brittle materials will change behavior and become ductile[27]. The transition temperature is called the brittle-ductile temperature: T_{BDT}. For SiC (4H) the T_{BDT} is found to be around 1600 Kelvin.[28] We will test the nanowires at 1600 Kelvin and see if we can see any ductile behavior such as necking and dislocations before failing. Ductile fracturing is interesting to study, because by analyzing the dislocations we can obtain knowledge about the slip systems in the material.

At high temperatures, the atoms will show random fluctuating motions due to the high kinetic energy. To make the interpretation of the results easier, we will filter out this random motion by performing a time average on the atoms. We sample the atoms at 100 time steps and print the mean values of their position, stress, and potential energy to the output data file. By doing this, we can simulate systems at high temperatures, while only investigating the consistent changes in positions, stress and potential energy due to the applied mechanical loading.

Mechanical properties of the polytypes

Figure 6.7 shows the stress-strain curves obtained from the tensile testing. Table 6.4 lists the mechanical properties obtained from the testing. Comparing these values with what is found in the literature is not easy, because no studies on the mechanical properties of SiC (2H) and (4H) nanowires could be found. However, the Young's modulus for bulk

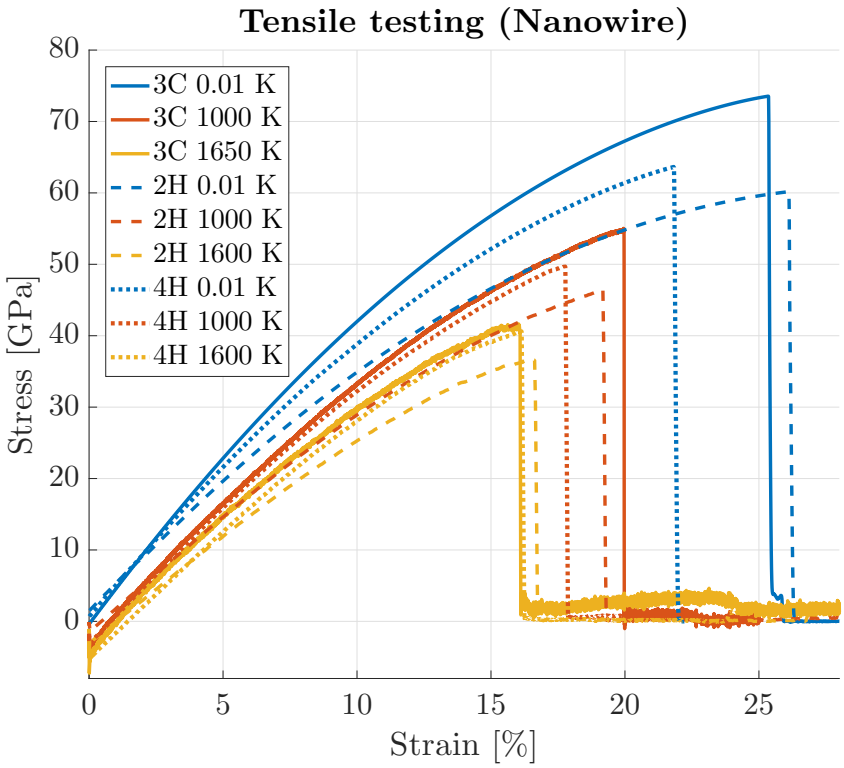

Figure 6.7: Stress-strain curves for the three polytypes at different temperatures. Please note that a smoothing function is used to smoothen out the high temperature curves.

SiC (2H) and SiC (4H) have been calculated using first principles and were found to be 441 GPa and 444 GPa[29], which is fairly close to the values obtained in this report.

In figure 6.8a, we see how the Young's modulus of each polytype depends on the temperature. We see that the Young's modules lower as the temperature increases. This is a known effect and is due to the fact that most materials loose stiffness at high temperatures.[30] Furthermore, we see that the (3C) polytype (0% hexagonality) has the highest Young's modulus, while the (2H) polytype (100% hexagonality) has the lowest values. Interestingly, the (4H) polytype (50% hexagonality), which can be seen as a fifty-fifty mixture of the (3C) and (2H) polytypes, lies roughly in middle of the two other polytypes. If more polytypes of different hexagonality had been simulated, it would be interesting to see if they lie in between the (3C) and (2H) polytypes according to their hexagonality. A study by B. Wen et al. confirms that this kind of dependency on the hexagonality exists in diamond polytypes.[31]

In 6.8b, we see a similar pattern: the maximum tensile stress before fracture decreases as the temperature increases, and the maximum stress of the (4H) polytype lies in between the (3C) and (2H) polytype.

When comparing the fracture strain (see figure 6.8c), we find that the (4H) polytype fractures at the lowest strain, while polytypes (2H) and (3C) have the highest and second highest fracture strain respectively. Looking at figure 6.9 (a-c), we see the difference in surface structure between the polytypes. We hypothesize that the zig-zag pattern of the (4H) polytype offers more sites of which fractures can occur, and therefore has a lower fracture strain. This fits with our discussion on the lower fracture strain of {11-2} surfaces compared to {1-10} surfaces, where the multiple dents and protrusions are thought to make it easier for fractures to occur.

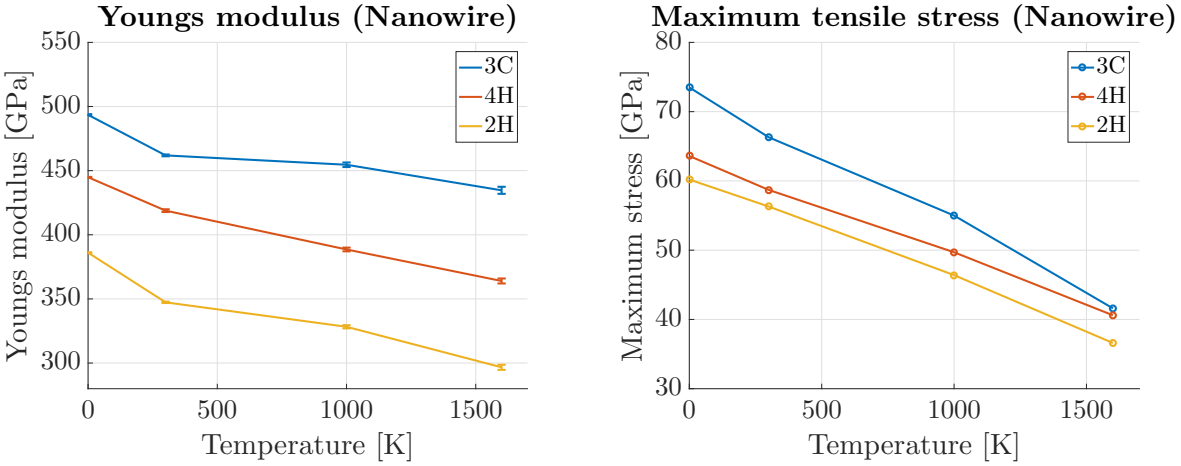

(a) Young's modulus.

(b) Maximum stress.

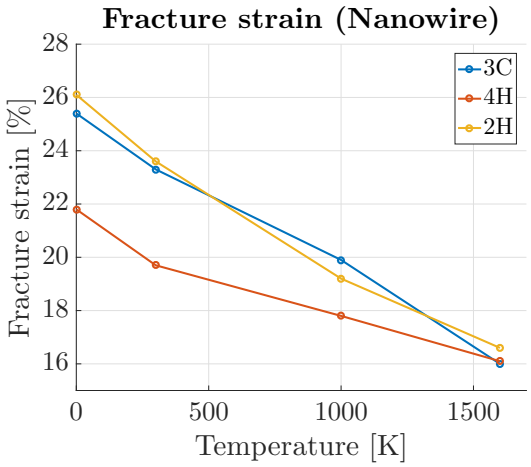

(c) Fracture strain.

Figure 6.8: Young's modulus, maximum stress, and fracture strain for the three polytypes at different temperatures.

Potential	Polytype /Radius	Temperature [K]	Young's modulus [GPa]	Tensile Strength [GPa]	Fracture Strain [%]
meam	2H/ 26Å	0.01	381.1 ± 0.3	60.2	26.1
		300	347.3 ± 0.5	56.3	23.6
		1000	328.3 ± 1.2	46.4	19.2
		1600	296.7 ± 2.0	36.6	16.6
	3C/ 25Å	0.01	493 ± 0.6	73.5	25.4
		300	461 ± 0.7	66.3	23.3
		1000	454.6 ± 1.8	55.0	19.9
		1650	434.7 ± 2.8	41.6	16.03
	4H/ 26Å	0.01	444.9 ± 0.3	63.6	21.8
		300	418.8 ± 1.1	58.7	19.7
		1000	388.6 ± 1.5	49.7	17.8
		1600	364.0 ± 1.9	40.6	16.14

Table 6.4: Mechanical properties for the three polytypes at different temperatures.

Fracture behavior of the polytypes

We want to examine if there is any difference in the fracture behavior of the three different polytypes. Figure 6.9 shows a side by side comparison of the fracturing of the polytypes at 1000 Kelvin. It can be seen that all polytypes show mode I fractures: as the crack propagates through the nanowire, we see a cleavage parallel to the direction of the applied tensile stress (see e.g. figures j-l) and the plane of the crack is normal to the applied stress. Mode I fracturing are a characteristic of brittle materials.

From figure 6.9, we see that from the fracture starts and until we have a fully fractured nanowire, only 0.015%-0.020% strain needs to be applied. This leads us to believe that the SiC nanowire exhibits unstable crack growth, meaning that the energy released by the initial fracture is higher than the energy required to create two surfaces. This will cause a chain reaction resulting in a complete rupture of the nanowire as soon as the first crack appears. Unstable crack growth is also a sign of a brittle material.

At all the temperatures we tested, the polytypes showed brittle fracture behavior. There were no signs of necking in the wires and no dislocations occurring before the fracturing, which would have been signs of a ductile fracture. Due to the limited time available for this work, we were not able to perform new tests at higher temperatures.

6.4 Interfaces of SiC on Si in nanowire heterostructure

In many semiconductor devices today, heterostructure components, where two semiconductor materials with different capabilities are grown together, play a major role. Heterostructures are found in various devices, such as transistors and semiconductor lasers. If the difference in lattice parameters of the two materials is too large, misfit dislocations will occur. Since dislocations generally will lower the performance of the device, it is an important research topic for scientists.

Misfit dislocations in nanowire heterostructures have previously been studied, for example in the 2006 paper by F Glas.[8] In this report we will use MD simulations to simulate a Si-SiC heterostructure with misfit dislocation. We make two heterostructures, one with SiC (3C) polytype and one with SiC (2H) polytype.

We construct the nanowire heterostructure such that the diameter is the same in both halves of the structure. Due to the difference in lattice parameters, the interface will be incoherent, meaning that it will contain a different number of atoms on each side. This creates misfit dislocations in the interface.

Using the minimization method described in the method section, we will ensure that the nanowire is in equilibrium before we start the analysis. We want to compare the potential energy of the interface to the two single crystal parts of the nanowire and analyze the dislocations forming at the interface.

Potential energy of the heterostructure

To compare the potential energy in the heterostructure, we take samples in three regions: one sample in the SiC material, one in the Si material, and one in the interface between the two materials. The regions are roughly illustrated in figure 6.10a. The regions of the SiC and Si samples cover one unit cell, since the potential energy might vary for each

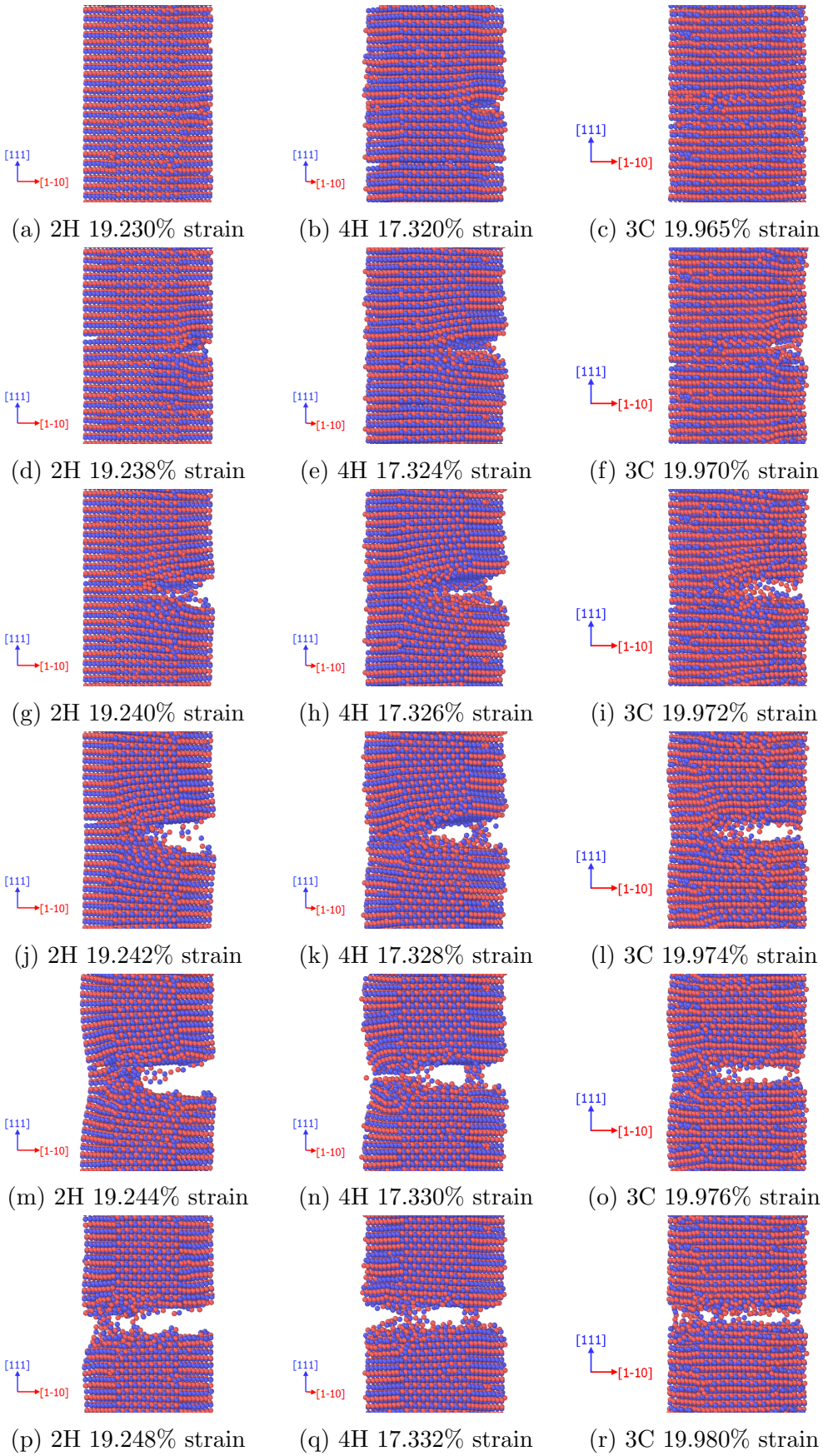

(a) 2H 19.230% strain (b) 4H 17.320% strain (c) 3C 19.965% strain

(d) 2H 19.238% strain (e) 4H 17.324% strain (f) 3C 19.970% strain

(g) 2H 19.240% strain (h) 4H 17.326% strain (i) 3C 19.972% strain

(j) 2H 19.242% strain (k) 4H 17.328% strain (l) 3C 19.974% strain

(m) 2H 19.244% strain (n) 4H 17.330% strain (o) 3C 19.976% strain

(p) 2H 19.248% strain (q) 4H 17.332% strain (r) 3C 19.980% strain

Figure 6.9: Mode I fractures of SiC (2H), (4H), and (3C) nanowires at 1000 Kelvin.

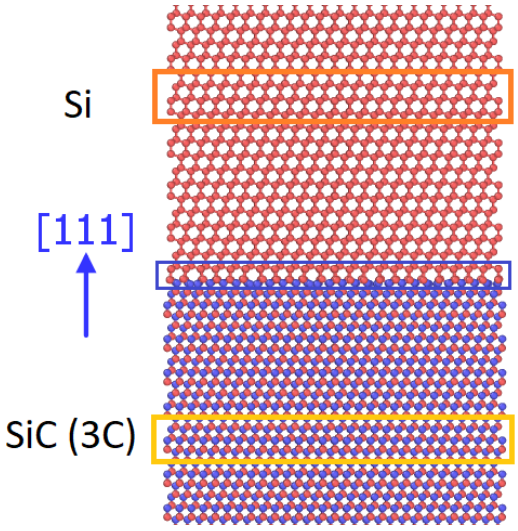

(a) Si-SiC (3C) heterostructure.

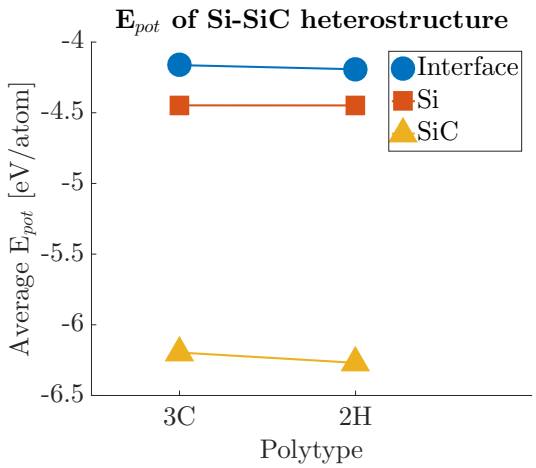

(b) Average potential energy in the three regions indicated in (a).

Figure 6.10: Part (a) shows a nanowire heterostructure of Si and SiC (3C). The three rectangles marks the regions: Si, interface, and SiC (3C) where the average potential energy was sampled. Part (b) shows the average potential energy per atom in each region for both SiC (3C) and SiC (2H) heterostructures.

bi-layer of atoms, but remain the same for each unit cell. For the interface sample, the region covers the first layers of atoms in the Si and SiC materials.

The average potential energy obtained is shown in figure 6.10 for both Si-SiC (3C) and Si-SiC (2H) heterostructures. The interface has higher potential energy than both the Si and SiC sections of the structures. This is explained by the misfit dislocations occurring at the interface.

In figure 6.11, cross sectional views of the interface are shown. Figures on the left show the SiC side of the interface, while figures on the right show the Si side of the interface. A periodic pattern in the atoms of higher potential energy is seen.

We see that the six-fold rotational symmetry in the radial direction is broken at the interface. In the SiC (3C) interface (figure 6.11a), we see a three-fold rotational symmetry: if we situate ourselves at the center of the hexagon looking towards one of the side facets, we would have to rotate 120° about our own axis to see the same potential energy landscape. For the SiC (2H) interface the rotational symmetry is completely broken. Instead we see a pattern of horizontal lines, where not even two fold symmetry is present due to one misaligned atom.

Since the symmetries in crystal structures affect the electron band structure, we would expect differences in band structure of the interfaces compared to the pure material sections of the heterostructure. To investigate the full consequences of this is beyond the scope of this report.

Dislocations in the heterostructure interface

Using the dislocation analyzer tool, DXA, in Ovito, we analyzed both the crystal structure and dislocation types forming in the interface of a heterostructure. Figure 6.12 illustrates how the DXA tool works. The figure shows a cut-through of a Si-SiC(2H) nanowire. The orange color indicates Wurtzite crystal structure and the blue color indicates diamond cubic/Zinc-blende crystal structure. The gray color indicates atoms for which no

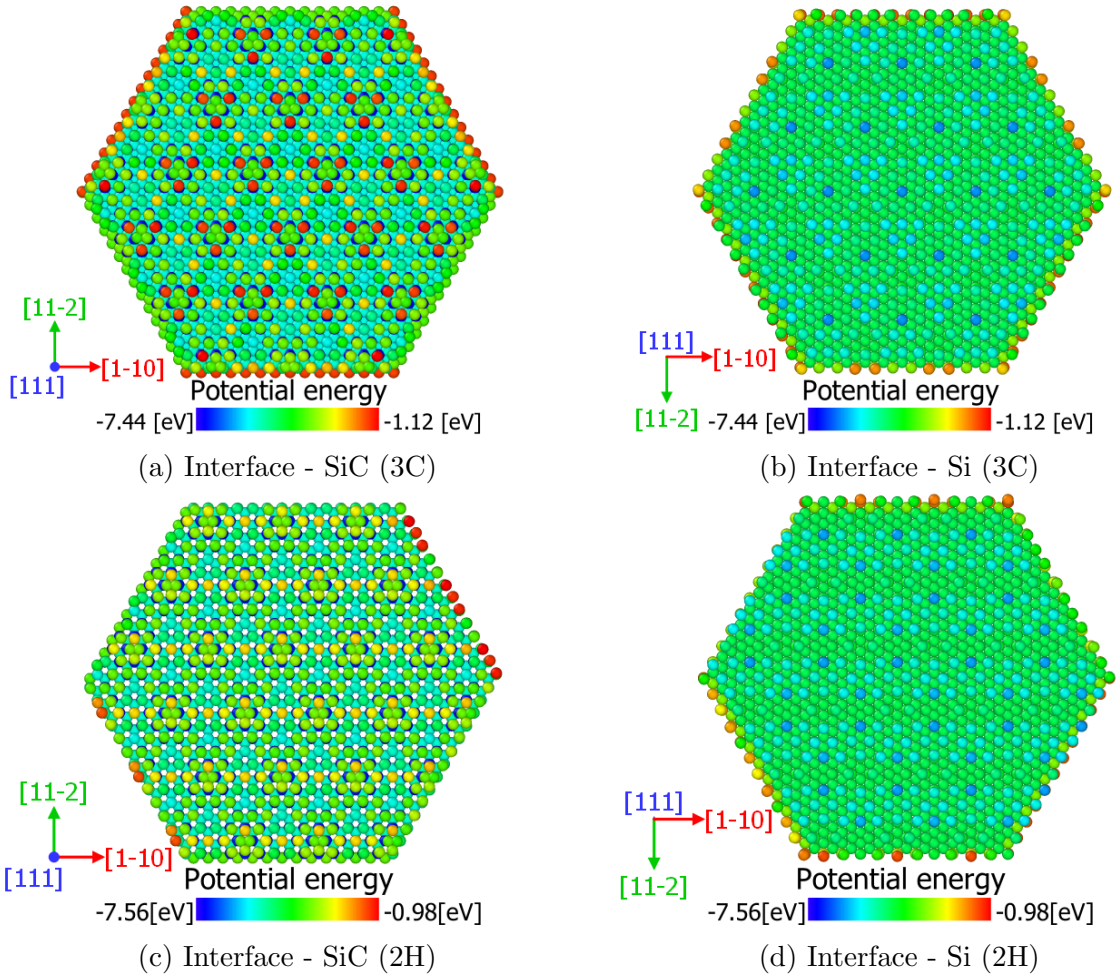

(a) Interface - SiC (3C)

(b) Interface - Si (3C)

(c) Interface - SiC (2H)

(d) Interface - Si (2H)

Figure 6.11: Cross sections of the interface showing the potential energy.

periodic crystal structure could be found. The surface atoms are gray due to their missing neighbors, but also in the interface gray atoms are present as a result of the misfit dislocations.

Figure 6.13 shows a cross sectional view of the interface. Again, orange particle color represents Wurtzite crystal structure, blue is Zinc-blende, and gray is for atoms that do not match a periodic crystal structure.

The green and blue lines are the dislocation lines. Green lines represent dislocations of the type $\frac{1}{6}\langle 11\text{-}2\rangle$ Shockley partial dislocations and blue lines are $\frac{1}{2}\langle 1\text{-}10\rangle$ perfect dislocations. Both dislocation types are known to appear in material of diamond crystal structures.[32] We see multiple cases of perfect dislocations dissociating into two partial dislocations, which is a known effect.[32] Red lines are dislocations that could not be matched to any known dislocation type. These appear only at the edges and could be because the diameters of the two parts of the heterostructure do not match perfectly.

In the 2006 paper by F. Glas, the formation of misfit dislocations in nanowire heterostructures is studied. Here it was assumed that 60° dislocation would form at the interface since it is a common dislocation type in fcc materials. 60° dislocations are characterized by the Burgers vector forming a 60° angle with the direction of the dislocation line.

In our simulation we do not find any 60° dislocations, only edge dislocations where the Burgers vector form a 90° angle with the dislocation line. All Burgers vectors and

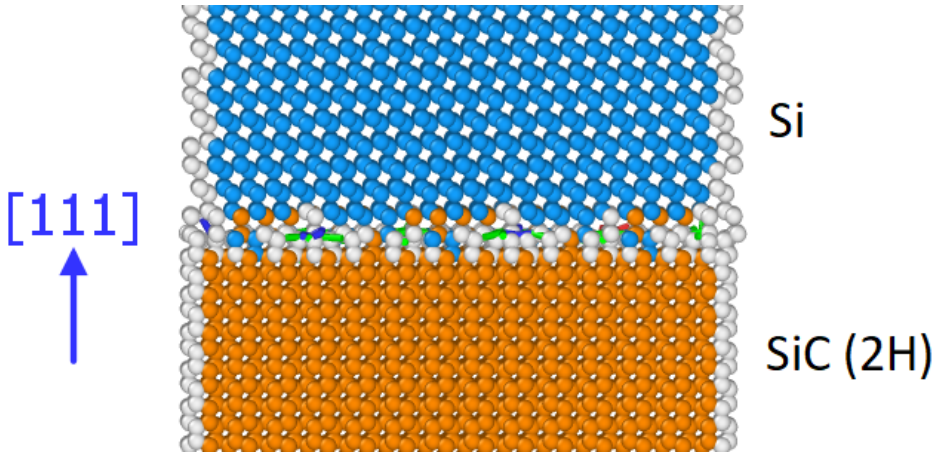

Figure 6.12: Cross section of a nanowire heterostructure of Si and SiC (2H) visualized using the DXA tool in Ovito. The blue particle color indicates diamond cubic/Zinc-blende, the orange color Wurtzite structure, and the grey color is atoms that couldn't be assigned any know periodic crystal structure. In the interface, dislocation lines can be seen.

dislocation lines lie in the xy-plane. This is not surprising since the (111) surface is the plane of highest lattice site density in both Zinc-blende and Wurtzite crystal structures and is therefore a preferred slip plane.[32]

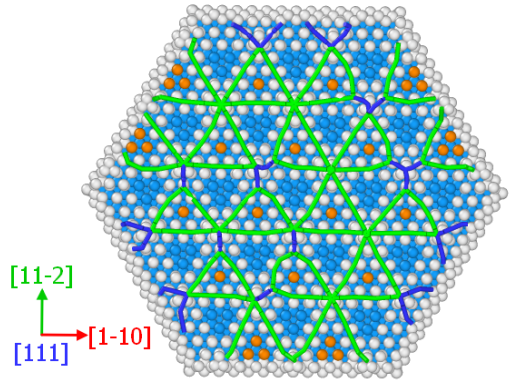

(a) SiC (3C) interface: dislocations and crystal structure

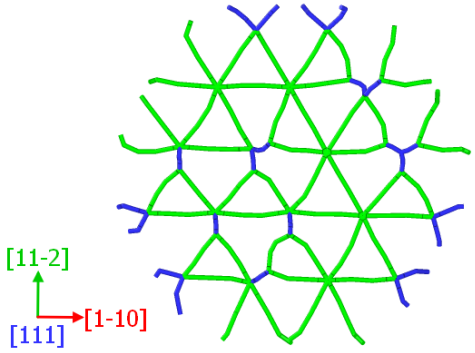

(b) SiC (3C) interface: dislocation lines

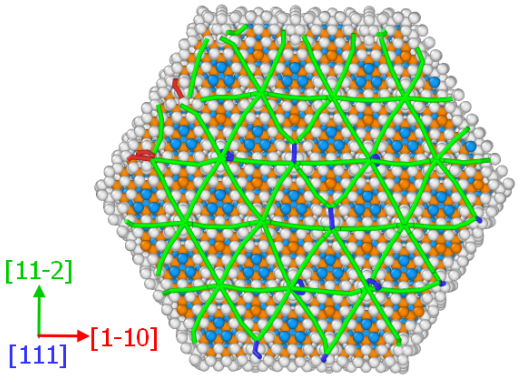

(c) SiC (2H) interface: dislocation and crystal structure

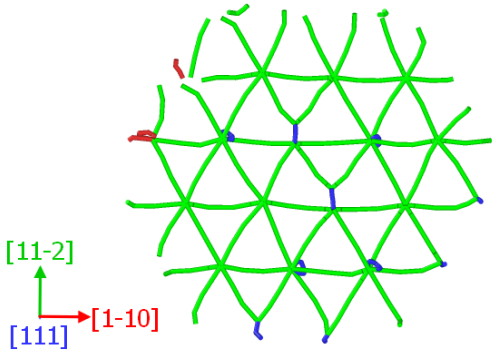

(d) SiC (2H) interface: dislocation lines

Figure 6.13: Dislocation lines and crystal structure in the interface.

Conclusions and Outlook

7.1 Conclusions

SiC nanowires may prove to be the ideal building block for creating highly specialized devices. However, in order to fully utilize them, their mechanical properties need to known.

In this report, MD simulations were used to obtain the mechanical properties of three SiC polytypes: (2H), (3C), and (4H). A side-by-side comparison was made of three commonly used inter-atomic potentials: the Vashishta, the Tersoff and the MEAM potential. It was found that for the original cut-off parameters in the Tersoff potential the cut-off function, f_{cut}, would affect the result of the tensile testing. This has been documented by others as well.[21] Therefore a new, larger cut-off parameter, R, was chosen in order to avoid interaction within the cut-off region. The Vashishta and the MEAM potentials did not show this kind of problem.

Tests on samples of bulk and nanowire SiC (3C) were performed in order to compare the mechanical properties predicted by the three potentials. The obtained values were compared with values found in literature. We also compared how the potentials predict the fracturing of the samples. For the nanowire samples both the Tersoff and the Vashishta potentials showed unexplained surface effects. The MEAM potential predicted mechanical properties that were close to those found in literature and it showed a predictable fracturing of both the bulk and nanowire sample. Therefore the MEAM potential was chosen for the following experiments.

By changing the orientation of the crystal lattice, we constructed two similar-sized nanowires with different side facets: one with {11-2} surfaces and one with {1-10} surfaces. We found a simple method for estimating the surface energy and compared it to values found in literature. It was found that the type of surfaces will affect the mechanical properties of the nanowire. Differences in the surface structure and stiffness were used to explain this.

Tensile testing of three nanowires with different polytypes was performed at four different temperatures. The mechanical properties of the polytypes were obtained, and we found a dependency of the Young's modulus on the hexagonality of the unit cell. This dependency has also been documented for diamond polytypes in the literature.[31]

We found that the values of the mechanical properties will decrease as the temperature increases. The difference between the fracture strain of the three polytypes was decreasing for high temperatures.

Lastly, two nanowire heterostructures were created using diamond cubic Si and the two polytypes: SiC (3C) and SiC (2H). We obtained the potential energy of the heterostructure interfaces and found it was higher than the potential energy of the pure Si and SiC parts of the nanowire. The occurrence of misfit dislocations in the interface explains this difference. The dislocation pattern of the two interfaces was analyzed, and we found edge dislocations

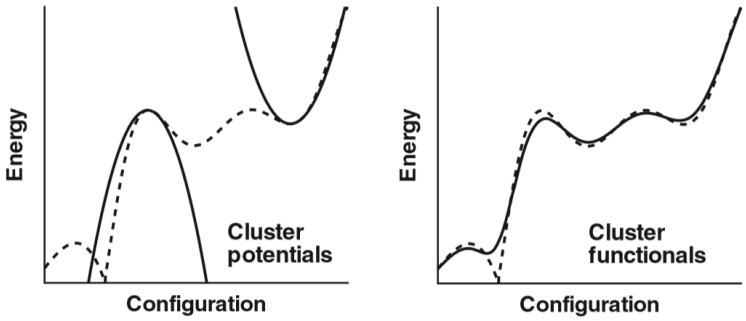

Figure 7.1: Graphical representation of cluster potentials and cluster functionals. The dashed line is the energy model by DFT. *(Reproduced from Modeling Materials by E. Tadmor and R. Miller[3, Fig 5.7 pp 282])*

of the types $\frac{1}{2}\langle$1-10$\rangle$ perfect dislocations and $\frac{1}{6}\langle$11-2$\rangle$ Shockley partial dislocations in the interface. The dislocation lines and their Burgers vectors all lie in the xy-plane. We did not find any 60° dislocations, which otherwise has been assumed to exist in the interface.

7.2 Discussion

It is important to note that the results obtained in MD simulations are only as good as the prediction of the inter-atomic model. Since most potentials are fitted to model certain aspects of a material, it is useful to introduce the concept of transferability.

The transferability of an inter-atomic model refers to how well the model is able predict the behavior of the material outside of the region to which it was originally fitted.[3, p 282-284] Quantifying the term transferability is not easily done, instead we will illustrate the concept by reproducing a schematic drawing created by A. E. Carlsson in figure 7.1.[33][3]

In figure 7.1 the energy is shown as a function of the configuration, which is the spatial positions of each individual atom in the structure. The dashed line represents the exact energy, as modeled by density functional theory (DFT), and it is a very complex function of the configuration. Cluster potentials are usually designed to model a small local configuration of the material, e.g. near the melting point of a solid. As long as they do not stray too far away form this initial configuration, they can accurately model the behavior of the material. However, outside the fitted region the result may differ from the real energy. As the figure illustrates, the same cluster potential fitted at two different local configurations may differ a lot from each other and therefore predict very different energies of the same configuration.

Cluster functionals are expressed in a more general formalism than cluster potentials and are therefore able to model a much broader range of configurations, as seen in figure 7.1.[3, p 283] However it is not likely that a cluster functional is able to reproduce the exact energy as found by DFT. Cluster functionals are able to provide a good global fit, but fine details in the energy function will be lost[3, pp283].

This offers an explanation to how the three potentials used in this report can predict very different mechanical properties even though all of them were fitted to model the same material. It also raises the question of how we can validate the results predicted by

the potentials. Comparisons with real-life experiments were not an option for us, since SiC nanowires are rarely found as single polytypes and tensile testings of nanowires, in general, are hard to perform due to their small size. Instead, validation was made by comparing with simulations done by other researchers and by analyzing the behavior of the nanowires, such as the fracturing, to see if it corresponds to what is found in the literature.

Even though validation can be difficult, results obtained through MD simulations are still very useful to the field of material science, because it allows us to perform mechanical test on systems that otherwise would be impossible to do experimentally. However, it is important to remember that the results obtained through MD simulations are only as accurate as the inter-atomic potential allows them to be.

7.3 Outlook

Our report has covered multiple aspects of the three SiC polytype nanowires: we have obtained mechanical properties, analyzed the fracture behavior, estimated the surface energies for the two surface types, and created Si-SiC heterostructures. Future work could therefore take many directions.

An obvious way to go would be to include more polytypes in our tests. Especially the SiC (6H) polytype, also known as β-SiC would be interesting to include since it is a very common polytype found in SiC. Its unit cell has a hexagonality of 33.3%. If our theory of a directed dependency of Young's modulus and the hexagonality is correct, the Young's modulus of SiC (6H) should lie between SiC (4H) and SiC (3C).

If we performed tensile testing at higher temperatures we might be able to see ductile fracture behavior in the SiC polytypes. Through analyzing the dislocation occurring in the ductile fracturing, we would obtain knowledge about the slip systems in the polytypes. By comparing the polytypes, we would see if there is any difference in the preferred slip planes.

During our studies, we found a simple way of estimating the surface energies. Using this method to measure the difference in surface energies of the three polytypes would be interesting, since it might help researchers in their studies on how growth conditions favors the growth of certain polytypes.

Lastly, an in-depth study of the polytype interfaces in nanowires would be highly relevant, since SiC nanowires grown today typically exhibit multiple polytypes in the same nanowire.[6] Using the techniques in this report, we can investigate how the interfaces of different polytypes will affect the mechanical properties of the nanowires. We could adapt a quantum mechanical modeling technique, such as DFT, and get a very precise model of the interfaces between polytypes.

Bibliography

[1] Yat Li et al. "Nanowire electronic and optoelectronic devices". In: *Materials Today* (2006).

[2] K Zekentes and K Rogdakis. "SiC nanowires: material and devices". In: *J. Phys. D: Appl. Phys.* 44 (2011), p. 133001.

[3] Ellad B Tadmor and Ronald E Miller. *Modeling Materials: Continuum, Atomistics and Multiscale Techniques*. Cambridge CB2 8RU UK: Cambridge University Press, 2011. ISBN: 978-0-521-85698-0.

[4] *LAMMPS Documentation*. Sandia Corporation. 2019. URL: `https://lammps.sandia.gov/doc/Manual.html`.

[5] Tesfaye Ayalew. *SiC Semiconductor Devices Technology, Modeling, and Simulation*. TU Wien - Institute for Microelectronics. 2004. URL: `http://www.iue.tuwien.ac.at/phd/ayalew/node20.html`.

[6] Lunet E. Luna et al. "Demonstration of Hexagonal Phase Silicon Carbide Nanowire Arrays with Vertical Alignment". In: *Crystal Growth and Design* 16 (2016), pp. 2887–2892.

[7] Y. Yao, S. T. Lee, and F. H. Li. "Direct synthesis of 2H–SiC nanowhiskers". In: *Chemical Physical Letters* 381 (2003), pp. 628–633.

[8] Frank Glas. "Critical dimensions for the plastic relaxation of strained axial heterostructures in free-standing nanowires". In: *Physical Review B* 74 (2006), p. 121302.

[9] W. H. Backes. "On the band gap variation in SiC polytypes". Ph.D. Thesis. Technische Universiteit Eindhoven, 1996.

[10] William J. Percibali. "Ceramicarmor Apparatus for Multiple Bullet Protection". Pat. US 6,408,733 B1. URL: `https://patents.google.com/patent/US6408733B1/en`.

[11] *Silicon Carbide as Armor Material*. Saint-Gobain High-Performance Refractories. URL: `https://www.azom.com/article.aspx?ArticleID=15534`.

[12] H. Föll. *Ramsdell Notation for SiC Polytypes*. Technische Fakultät - CAU Kiel. URL: `https://www.tf.uni-kiel.de/matwis/amat/semi_en/kap_a/basics/ba_1_1.html`.

[13] P. Vashishta et al. "Interaction potential for silicon carbide: A molecular dynamics study of elastic constants and vibrational density of states for crystalline and amorphous silicon carbide." In: *Journal of Applied Physics* 101 (2007), p. 103515.

[14] J. Tersoff. "New empirical model for the structural properties of silicon." In: *Physics Review Letter* 56 (1986), pp. 632–635.

[15] P. M. Gullet, P. Wagner, and M. Slepoy. *Numerical Tools for Atomistic Simulations*. Report. Sandia National Laboratories, 2003. DOI: `SAND2003-8782`. URL: `infoserve.sandia.gov/sand_doc/2003/038782.pdf`.

[16] Henggao Xiang, Haitao Li, and Xianghe Peng. "Comparison of different interatomic potentials for MD simulations of AlN". In: *Computational Materials Science* 140 (2017), pp. 113–120.

[17] J. Tersoff. "Modeling solid-state chemistry: Interatomic potentials for multicomponent systems." In: *Physics Review B* 39 (1989), pp. 5566–5568.

[18] *OVITO - The Open Visualization Tool*. OVITO. 2019. URL: `http://www.ovito.org/`.

[19] Alexander Stukowski. *Dislocation analysis (DXA)*. Ovito. 2017. URL: `http://www.ovito.org/manual/particles.modifiers.dislocation_analysis.html`.

[20] *MATLAB*. MathWorks. 2019. URL: `https://se.mathworks.com/products/matlab.html`.

[21] X. W. Zhou and R. E. Jones. "Effects of Cutoff Functions of Tersoff Potentials on Molecular Dynamics Simulations of Thermal Transport". In: *Modeling and Simulation in Materials Science and Engineering* 19 (2011), p. 025004.

[22] Maxim A. Makeev, Deepak Srivastava, and Madhu Menon. "Silicon carbide nanowires under external loads: An atomistic simulation study". In: *Physical Review B* 74 (2006), p. 165303.

[23] Liming Xiong, Youping Chen, and James D. Lee. "Atomistic simulation of mechanical properties of diamond and silicon carbide by a field theory". In: *Modelling Simul. Mater. Sci. Eng.* 15 (2007), pp. 535–551.

[24] V.I.Ivashchenko, P. E. A. Turchi, and V. I. Shevchenko. "Simulations of the mechanical properties of crystalline, nanocrystalline, and amorphous SiC and Si". In: *Physical Review B* 75 (2007), p. 085209.

[25] Wen-Xiu Wang et al. "Tensile mechanical behaviors of cubic silicon carbide thin films". In: *Computational Material Science* 62 (2012), pp. 195–202.

[26] Eric K. K. Abavare et al. "Surface energy of Si(110)- and 3C-SiC(111)-terminated surfaces". In: *Physica Status Solidi B* 251 (2014), pp. 1408–1415.

[27] *Ductile to Brittle Transition*. UNSW Sydney. 2014. URL: `http://www.materials.unsw.edu.au/tutorials/online-tutorials/2ductile-brittle-transition`.

[28] Ming Zhang et al. "Transition from brittle fracture to ductile behavior in 4H–SiC". In: *Journal of Material Reseacrh* 18 (2011), pp. 1087–1095.

[29] Md. Nuruzzaman et al. "Structural, elastic and electronic properties of 2H- and 4H-SiC". In: *International Journal of Engineering Research and Applications* (2015), pp. 48–52.

[30] D. Zakarian, A. Khachatrian, and S. Firstov. "Universal temperature dependence of Young's modulus". In: *Metal Powder Report* online material (2019).

[31] Bin Wen et al. "First principle studies of diamond polytypes". In: *Diamond and Related Materials* 17 (2008), pp. 356–364.

[32] A. T. Blumenau et al. "Dislocation structures in diamond: density-functional based modelling and high resolution electron microscopy". In: *Defects and Diffusion in Ceramics* 226 (2004), pp. 11–30.

[33] A E Carlsson. "Beyound pair potentials in elemental transition metals and semiconductors." In: *Solid State Physics* 43 (1990), pp. 1–91.

The MEAM potential

In the MEAM potential, the energy is given by:

$$E = \sum_i \left[F_i\left(\overline{\rho}_i\right) + \frac{1}{2} \sum_{j(\neq i)} \phi_{ij}\left(r_{ij}\right) \right] \tag{A.1}$$

The pair potential ϕ_{ij} incorporates the screening function S_{ij} and the embedding function F_i, which will be described below. The general shape of the pair potential is determined by the exponential function $\exp(-a^*_{ij}(r^{ij}))$ which depends on the normalized distance function $a^*_{ij}(r^{ij})$:

$$\phi_{ij}\left(r_{ij}\right) = \overline{\phi}_{ij}\left(r_{ij}\right) S_{ij} \tag{A.2a}$$

$$\overline{\phi}_{ij}\left(r_{ij}\right) = \frac{1}{Z_{ij0}} \left[2E^u_i\left(r_{ij}\right) - F_i\left(\hat{\rho}_i\left(r_{ij}\right)\right) - F_j\left(\hat{\rho}_j\left(r_{ij}\right)\right) \right] \tag{A.2b}$$

$$E^u_i\left(r_{ij}\right) = -E^0_{ij}\left(1 + a^*_{ij}\left(r_{ij}\right)\right) e^{-a^*_{ij}(r_{ij})} \tag{A.2c}$$

$$a_{ij}\left(r_{ij}\right)^* = \alpha^0_{ij}\left(\frac{r_{ij}}{r^0_{ij}} - 1\right) \tag{A.2d}$$

The parameters E^0_{ij}, α^0_{ij}, and r^0_{ij} depend on the elements i and j. The parameter Z_{ij0} is the first nearest neighbor coordination of the reference structure of the system and the electron densities, $\hat{\rho}$, are calculated for the reference structure as well.

The functional term:

$$F_i\left(\overline{\rho}_i\right) = A_i E^0_i \overline{\rho}_i \ln \overline{\rho}_i \tag{A.3}$$

$$\overline{\rho}_i = \frac{\overline{\rho}^{(0)}_i}{\rho^0_i} G_i\left(\Gamma_i\right) \tag{A.4}$$

$$G_i = \sqrt{1 + \Gamma_i}\ , \qquad \Gamma_i = \sum_{k=1}^{3} t^{(k)}_i \left(\frac{\overline{\rho}^{(k)}_i}{\overline{\rho}^{(0)}_i} \right)^2 \tag{A.5}$$

$$\rho^0_i = \rho_{i0} Z_{i0} G_i\left(\Gamma^{ref}_i\right)\ , \qquad \Gamma^{ref}_i = \sum_{k=1}^{3} t^{(k)}_i \frac{s^{(k)}_i}{Z^2_{i0}} \tag{A.6}$$

Where $t^{(k)}_i$ is a weighting function given by:

$$t^{(k)}_i = \frac{1}{\overline{\rho}^{(0)}_i} \sum_{j \neq i} t^{(k)}_{0,j} \rho^{a(0)}_j S_{ij} \tag{A.7}$$

Where $t_{0,j}^{(k)}$ is a fitting parameter.

The electron densities are given by:

$$\overline{\rho}_i^{(0)} = \sum_{j \neq i} \rho_j^{a(0)}\left(r_{ij}\right) S_{ij} \tag{A.8a}$$

$$\left(\overline{\rho}_i^{(1)}\right)^2 = \sum_{\alpha=1}^{3} \left[\sum_{j \neq i} \rho_j^{a(1)} \frac{r_{ij\alpha}}{r_{ij}} S_{ij}\right]^2 \tag{A.8b}$$

$$\left(\overline{\rho}_i^{(2)}\right)^2 = \sum_{\alpha=1}^{3}\sum_{\beta=1}^{3} \left[\sum_{j \neq i} \rho_j^{a(2)} \frac{r_{ij\alpha} r_{ij\beta}}{r_{ij}^2} S_{ij}\right]^2 - \frac{1}{3}\left[\sum_{j \neq i} \rho_j^{a(2)}\left(r_{ij}\right) S_{ij}\right]^2 \tag{A.8c}$$

$$\left(\overline{\rho}_i^{(3)}\right)^2 = \sum_{\alpha=1}^{3}\sum_{\beta=1}^{3}\sum_{\gamma=1}^{3} \left[\sum_{j \neq i} \rho_j^{a(3)} \frac{r_{ij\alpha} r_{ij\beta} r_{ij\gamma}}{r_{ij}^3} S_{ij}\right]^2 - \frac{3}{5}\sum_{\alpha=1}^{3}\left[\sum_{j \neq i} \rho_j^{a(3)} \frac{r_{ij\alpha}}{r_{ij}} S_{ij}\right]^2 \tag{A.8d}$$

The electron densities, $\rho_i^{a(k)}$, are a function of the distance from the atom:

$$\rho_i^{a(k)}\left(r_{ij}\right) = \rho_{i0} \exp\left[-\beta_i^{(k)}\left(\frac{r_{ij}}{r_i^0} - 1\right)\right] \tag{A.9}$$

Where ρ_{i0} and β_i are fitting parameters depending on the element.

The screening function, S_{ij}, takes values between 1 and 0. If there is a clear line of sight between two atoms i and j the screening function equals 1. If there is a third atom, k, in between the two atoms i and j obscuring the line of sight the value is 0. Intermediate values comes when the atom j is partially obscured by atom k.

The screening function also works as a cut-off function which go to 0 when the inter-atomic distance, r_{ij}, exceed the cut-off radius, r_c.

The function S_{ij} is given by:

$$S_{ij} = \overline{S}_{ij} f_c\left(\frac{r_c - r_{ij}}{\Delta r}\right) \tag{A.10a}$$

$$\overline{S}_{ij} = \prod_{k \neq i,j} S_{ikj} \tag{A.10b}$$

$$S_{ikj} = f_c\left(\frac{C_{ikj} - C_{\min,ikj}}{C_{\max,ikj} - C_{\min,ikj}}\right) \tag{A.10c}$$

$$C_{ikj} = 1 + 2\frac{r_{ij}^2 r_{ik}^2 + r_{ij}^2 r_{jk}^2 - r_{ij}^4}{r_{ij}^4 - \left(r_{ik}^2 - r_{jk}^2\right)^2} \tag{A.10d}$$

$$f_c(x) = \begin{cases} 1 & x \geq 1 \\ \left[1 - (1-x)^4\right]^2 & 0 < x < 1 \\ 0 & x \leq 0 \end{cases} \tag{A.10e}$$

Where C_{min} and C_{max} are fitting parameters and Δr is a length scale which determines the region in which S_{ij} goes from 1 to 0.

Inter-atomic potential parameters

B.1 Vashishta parameters

```
# DATE: 2015-10-14
#CONTRIBUTOR: Aidan Thompson, athomps@sandia.gov
#CITATION: P. Vashishta, R. K. Kalia, A. Nakano,
#and J. P. Rino. J. Appl. Phys. 101, #103515 (2007).

# Vashishta potential file for SiC, P. Vashishta, R. K. Kalia,
#A. Nakano, and J. P. Rino. J. Appl. Phys. 101, 103515 (2007).

# These entries are in LAMMPS "metal" units:
#   H = eV*Angstroms^eta; Zi, Zj = |e| (e = electronic charge);
#   lambda1, lambda4, rc, r0, gamma = Angstroms;
#   D = eV*Angstroms^4; W = eV*Angstroms^6; B = eV;
#   other quantities are unitless

#  Note: Value of D here equals D/2 in paper

# element1  element2  element3 H  eta  Zi  Zj  lambda1  D  lambda4
# W  rc  B  gamma  r0  C  cos(theta)

C   C    C  471.74538  7  -1.201  -1.201  5.0  0.0  3.0
0.0  7.35  0.0  0.0  0.0  0.0  0.0

Si  Si  Si  23.67291  7  1.201  1.201  5.0  15.575  3.0
0.0  7.35  0.0  0.0  0.0  0.0  0.0

C   Si  Si  447.09026  9  -1.201  1.201  5.0  7.7874  3.0
61.4694  7.35  9.003  1.0  2.90  5.0  -0.333333333333

Si  C   C   447.09026  9  1.201  -1.201  5.0  7.7874  3.0
61.4694  7.35  9.003  1.0  2.90  5.0  -0.333333333333

C   C   Si  0.0  0.0  0.0  0.0  0.0  0.0  0.0
0.0  0.0  0.0  0.0  0.0  0.0  0.0

C   Si  C   0.0  0.0  0.0  0.0  0.0  0.0  0.0
0.0  0.0  0.0  0.0  0.0  0.0  0.0
```

```
Si  C   Si  0.0  0.0  0.0  0.0  0.0  0.0  0.0
0.0  0.0  0.0  0.0  0.0  0.0  0.0

Si  Si  C   0.0  0.0  0.0  0.0  0.0  0.0  0.0
0.0  0.0  0.0  0.0  0.0  0.0  0.0
```

B.2 Tersoff parameters

```
# DATE: 2011-04-26
#CONTRIBUTOR: Aidan Thompson, athomps@sandia.gov
#CITATION: Tersoff, Phys Rev B, 39, 5566-5568 (1989)
#DATE: 2019-04-15: Parameter R for SiC interaction modified
#by Anders Vesti

# Si and C mixture, parameterized for Tersoff potential
# this file is from Rutuparna.Narulkar @ okstate.edu
# values are from Phys Rev B, 39, 5566-5568 (1989)
# and errata (PRB 41, 3248)

# Tersoff parameters for various elements and mixtures
# multiple entries can be added to this file, LAMMPS reads the ones
# it needs. these entries are in LAMMPS "metal" units:
#   A,B = eV; lambda1,lambda2,lambda3 = 1/Angstroms; R,D = Angstroms
#   other quantities are unitless.

# format of a single entry (one or more lines):
# element 1, element 2, element 3, m, gamma, lambda3, c, d, costheta0,
# n, beta, lambda2, B, R, D, lambda1, A

C   C    C   3.0 1.0 0.0 38049  4.3484   -.57058 .72751
0.00000015724 2.2119  346.7   1.95   0.15   3.4879  1393.6

Si  Si  Si  3.0 1.0 0.0  100390  16.217   -.59825 .78734
0.0000011     1.73222  471.18  2.85   0.15    2.4799  1830.8

Si  Si  C   3.0 1.0 0.0 100390  16.217   -.59825 0.0
0.0 0.0 0.0 2.36   0.15 0.0 0.0

Si  C   C   3.0 1.0 0.0 100390 16.217 -.59825 .787340
0.0000011     1.97205 395.126  3.10  0.15    2.9839  1597.3111

C   Si  Si  3.0 1.0 0.0 38049  4.3484  -.57058 .72751
0.00000015724 1.97205 395.126  3.10  0.15   2.9839   1597.3111

C   Si  C   3.0 1.0 0.0 38049  4.3484   -.57058 0.0
0.0 0.0 0.0 1.95   0.15 0.0 0.0
```

```
C   C   Si  3.0 1.0 0.0 38049  4.3484   -.57058 0.0
0.0 0.0 0.0 2.36   0.15 0.0 0.0

Si  C   Si  3.0 1.0 0.0 100390 16.217 -.59825 0.0
0.0 0.0 0.0 2.85   0.15 0.0 0.0
```

B.3 Meam parameters

```
# DATE: 2007-06-11
# CONTRIBUTOR: Greg Wagner, gjwagne@sandia.gov

lattce(1,2) = 'dia'
Ec(1,2) = 6.4325
alpha(1,2) = 4.37
re(1,2) = 1.8878
rho0(2) = 2.25
rc = 4.0
delr = 0.1
Cmax(1,2,1) = 4.0
Cmax(1,2,2) = 4.0
Cmax(2,2,1) = 4.0
Cmax(1,1,2) = 4.0
```

Example of an input file

C.1 SiC (3C) nanowire using MEAM potential

```
#---Zincblende SiC (3C) nanowire---

units metal
dimension 3
boundary p p p
atom_style atomic

#---Lattice constants
variable latconst_a equal 4.3596
variable latconst_c equal sqrt(3)*latconst_a
variable c_3C equal sqrt(3)

#---Change radius of nanowire---
variable rad_p equal 4.0
variable rad_n equal -1*${rad_p}
variable height equal 6*${c_3C}

#---Geometric constants dependent on radius---
variable SiC_yp equal sqrt(3)/2*${rad_p}
variable SiC_yn equal sqrt(3)/2*${rad_n}
variable SiC_xp equal 0.5*${rad_p}
variable SiC_xn equal 0.5*${rad_n}

#---Create simulation box---
lattice fcc ${latconst_a}
region simbox block -5 5 -5 5 -0.01 ${height}
create_box 2 simbox

#---Defining nanowire ---
region nprism1 &
prism 0 ${rad_p} -0.01 ${SiC_yp} -0.01 ${height} ${SiC_xn} 0 0
region nprism2 &
prism ${rad_n} 0 -0.01 ${SiC_yp} -0.01 ${height} ${SiC_xp} 0 0
region nprism3 &
prism ${SiC_xn} ${SiC_xp} ${SiC_yn} -0.01 -0.01 ${height} ${SiC_xn} 0 0
region nprism4 &
prism ${SiC_xn} ${SiC_xp} ${SiC_yn} -0.01 -0.01 ${height} ${SiC_xp} 0 0
```

```
region         nanowire union 4 nprism1 nprism2 nprism3 nprism4


#---Creating the zb lattice (normalized z[111]-direction)
lattice        custom ${latconst_a} &
orient x 1 1 -2 orient y -1 1 0 orient z 1 1 1 &
a1 1.0 0.0 0.0 &
a2 0.0 1.0 0.0 &
a3 0.0 0.0 1.0 &
basis 0.0 0.0 0.0        basis 0.0 0.5 0.5 &
basis 0.5 0.0 0.5        basis 0.5 0.5 0.0 &
basis 0.25 0.25 0.25        basis 0.25 0.75 0.75 &
basis 0.75 0.25 0.75        basis 0.75 0.75 0.25

#---Adding atoms---
create_atoms 2 region nanowire &
basis 1 1 basis 2 1 basis 3 1 basis 4 1 &
basis 5 2 basis 6 2 basis 7 2 basis 7 2

group nanowire region nanowire

#---Defining Atomic potential---
mass        1        28.085
mass        2        12.011
group Si type 1
group C  type 2

pair_style        meam/c
pair_coeff        * * library.meam Si C SiC.meam Si C

#---Initial velocities
velocity        all create 0.01 511124 rot yes mom yes

#---Compute stress---
compute stress all stress/atom NULL
compute stress3 all reduce sum c_stress[3]
variable        stress equal c_stress3
variable        volu equal vol
variable        Lx equal lx
variable        Ly equal ly
variable        Lz equal lz
compute epatom all pe/atom
variable epot equal pe

#---Print to screen---
thermo     100
thermo_style    custom step vol temp pe  lx ly lz pzz c_stress3
```

```
#---Bar stat---
timestep   0.0001
fix         RELAXBOX all box/relax iso 0.0
min_style sd
minimize 1e-25 1e-25 50000 100000
unfix RELAXBOX


#---LOADING OF NANOWIRE---

#---Timeintegration---
fix        NVT all nvt temp 0.01 0.01 0.1

#----Start loading, strain rate 1e8 (1e-4)---
fix        LOAD nanowire deform 1 z erate 0.0001 units box

#---dump data to files----
dump 1 all custom 1000 SiC_3C.relax id type x y z c_stress[3] c_epatom
dump_modify 1 append yes

fix 1 all print 1000 "${stress} ${epot}" file SiC_3C.txt screen no

#----Screen output----
thermo     100
thermo_style    custom step vol temp pe lx ly lz pzz c_stress3

#----MD run (Loading)-------
timestep   0.001
run        3000000

# SIMULATION DONE
print "All done"
```